Volume 8
Number 34
14 September 2020
Pages 17279–17830

Journal of Materials Chemistry A

Materials for energy and sustainability

rsc.li/materials-a

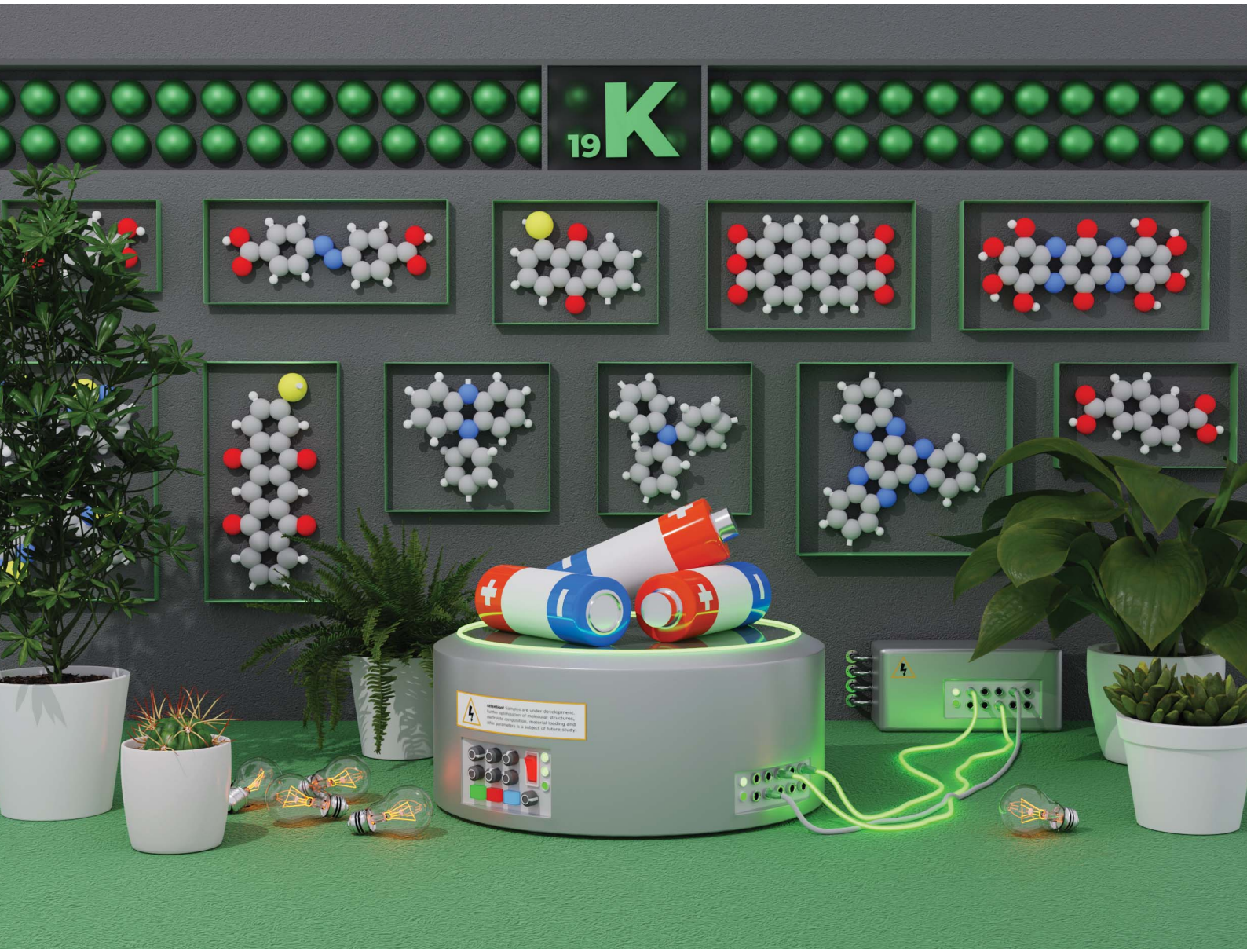

ISSN 2050-7488

ROYAL SOCIETY OF CHEMISTRY

REVIEW ARTICLE

Roman R. Kapaev and Pavel A. Troshin

Organic-based active electrode materials for potassium batteries: status and perspectives

Journal of Materials Chemistry A

REVIEW

View Article Online
View Journal | View Issue

Cite this: J. Mater. Chem. A, 2020, 8, 17296

Organic-based active electrode materials for potassium batteries: status and perspectives†

Roman R. Kapaev *[ab] and Pavel A. Troshin [ab]

If our demand for portable electronics and electric vehicles continues skyrocketing, lithium supplies, which are the basis for Li-ion batteries, might become scarce within several decades. Potassium-based batteries have recently attracted much attention as sustainable alternatives to Li-ion energy storage technologies. Potassium is a ubiquitous element, so its feedstocks are more than sufficient for extensive use in energy storage systems. It has been shown that potassium batteries might achieve high energy densities along with fast charge/discharge capabilities and superior cycling stability. Organic redox-active compounds have recently started to emerge as a promising class of materials for K-based batteries. They can be friendlier to the environment compared to inorganic alternatives and contain no expensive transition metals, which is crucial for sustainable development. For organic and metal–organic compounds, charge–discharge mechanisms are typically unspecific to the counter-ion, which makes the development of Li-ion battery alternatives easier. In this review, the recent progress of organic-based anode and cathode materials for potassium batteries is summarized. We define the main classes of redox-active compounds and their main challenges, analyze the performance of the materials compared to the best inorganic analogs, and reveal key strategies for improving energy density, rate capability and cycling stability.

Received 7th May 2020
Accepted 9th July 2020

DOI: 10.1039/d0ta04741d

rsc.li/materials-a

1. Introduction

Lithium-ion batteries (LIBs) revolutionized the field of energy storage devices owing to their high energy density, cycling stability and reliability.[1] There is a rapidly growing demand for such batteries in a multitude of applications, including portable electronics and electric vehicles.[2–4]

[a]Center for Energy Science and Technology, Skolkovo Institute of Science and Technology, Nobel Str. 3, Moscow 143026, Russia. E-mail: roman.kapaev@skoltech.ru
[b]Institute for Problems of Chemical Physics RAS (IPCP RAS), Acad. Semenov Ave. 1, Chernogolovka 142432, Russia

† Electronic supplementary information (ESI) available. See DOI: 10.1039/d0ta04741d

Roman Kapaev received his specialist degree in Chemistry from the Higher Chemical College of the RAS at the D. I. Mendeleev University of Chemical Technology in 2013. He is now a PhD student at the Skolkovo Institute of Science and Technology under the supervision of Prof. Pavel Troshin. His current research interests include materials for energy storage devices, such as metal–ion batteries.

Pavel Troshin graduated with a specialist degree from the Higher Chemical College of the RAS at the D. I. Mendeleev University of Chemical Technology. In 2006, he obtained his PhD from the Institute for Problems of Chemical Physics of the RAS. He is currently a full professor at the Skolkovo Institute of Science and Technology, and he is also a head of Laboratory of Functional Materials for Electronics and Medicine at the Institute for Problems of Chemical Physics of the Russian Academy of Sciences. His research interests include solar energy conversion, electrochemical energy storage, organic and molecular electronics, organic synthesis, and biomedical and fullerene chemistry.

However, the continuous growth of lithium consumption[5,6] raises concerns about the scarcity of its resources, which questions the sustainability of LIBs. Lithium is a rare element; its major feedstocks in the Earth's crust are concentrated only in a few countries, making the industry generally dependent on imports.[3,7] In some scenarios of LIB market expansion, the lithium supply might become insufficient during the next few decades.[8]

Besides lithium, a modern LIB typically contains non-widespread transition metals, such as copper (anode current collector), nickel and cobalt (cathode materials). The shortage in cobalt is especially acute. If cobalt-free batteries remain underdeveloped, the production of Co will have to increase up to an order of magnitude to satisfy the future demand.[3,9] Additionally, extraction and processing of transition metals might be harmful to the environment and is typically energy-intensive.[10]

The opportunity of making sustainable rechargeable batteries, which utilize only widespread elements, can be provided by using organic materials and replacing lithium by ubiquitous sodium or potassium. Particularly, potassium-based cells have recently attracted great attention, which can be seen from the rapidly growing number of papers dedicated to this topic (Chart S1†).

Potassium possesses similar chemical properties to lithium. The standard reduction potential for K is −2.93 V, which is close to that for Li (−3.04 V) and higher than for Na (−2.71 V); in propylene carbonate, the reduction potential for K is even lower than that for Li and Na.[11,12] The low anode potential helps to enhance voltage and energy density of the batteries. Graphite, which is a standard anode for LIBs, can be also used in potassium battery anodes, which is in contrast with sodium cells.[12–14] Owing to a weak Lewis acidity of potassium ions, diffusion coefficients of K^+ in electrolytes are higher than for Li^+ or Na^+, which is beneficial for fast charge–discharge.[15,16] For K-based batteries, cheaper and lighter aluminum can be used as the anode current collector instead of copper because potassium forms no alloys with Al.[17] Copper-free cells are also tolerant to over-discharge processes leading to the current collector dissolution in case of using copper, which are detrimental for cycling stability and may cause short-circuiting of LIBs.[9,17–20]

Organic materials have no toxic and expensive elements and can potentially be produced from renewable resources.[10,21–23] Redox chemistry of organic and metal–organic compounds is generally weakly dependent on the nature of counter-ions that balance excessive charges upon reduction/oxidation.[10,21] This is in contrast to inorganic battery materials, which usually rely on cation-specific complex intercalation mechanisms.[10,21] Such a versatility of organic-based compounds should make the development of alternative battery technologies easier since the same material can be successfully applied for lithium, sodium, potassium and other chemistries.

Although many reviews dedicated to potassium-based batteries have been published,[17,24–48] little emphasis has been laid on organic-based materials. This review aims to cover all reported organic and metal–organic active materials, as well as to compare them with state-of-the-art inorganic analogs in terms of capacity, voltage, energy, rate and cycle capabilities. In addition, key challenges and perspectives of the organic-based potassium batteries will be discussed. Since the materials were mostly investigated in non-aqueous cells (see Tables 1 and 2, structures are shown in Fig. 1 and 2), the focus of this review will be on water-free systems, although organic compounds for aqueous potassium batteries will also be discussed.

2. Cathode materials

2.1 Quinones and oxocarbon derivatives

Quinoid structures, especially 1,4-quinones, are currently the most studied family of organic redox-active cathode materials for potassium batteries. Quinone units undergo two-electron reversible reduction, as depicted in Scheme 1.[49–51] Salts of croconic acid ($H_2C_5O_5$) and rhodizonic acid ($H_2C_6O_6$), which may be considered oxocarbon derivatives, operate similarly, possessing up to two and four redox-active carbonyl groups, respectively.[49,52]

Small molecules. Simple low-molecular weight quinones, such as benzoquinone, naphthoquinone or anthraquinone, could be attractive because of their high theoretical capacity and low cost. Unfortunately, their high solubility in the electrolytes, which causes rapid capacity fading, makes them unsuitable.[53] One of the approaches to mitigate the dissolution problem is to introduce ionic substituents, such as $-SO_3Na$.

Anthraquinone-1,5-disulfonic acid disodium salt (1,5-AQDS, **1a**) was first proposed for potassium batteries by Xu *et al.*[54] In a carbonate-based electrolyte, the authors achieved the reversible capacity per material mass (Q_m) of 95 mA h g^{-1} at 0.1C (13 mA g^{-1}), and after a hundred cycles the capacity was 78 mA h g^{-1}.

Later, Xu *et al.*[55] investigated how the electrolyte affects the performance of **1a**-based cathodes. It was shown that a KFSI solution in 1,2-dimethoxyethane (DME) enables much better rate capability and cycling stability of 1,5-AQDS, owing to a stable solid electrolyte interphase (SEI) forming in this electrolyte. For the optimized electrolyte composition, Q_m was 84 mA h g^{-1} at 3C (390 mA g^{-1}), and 80% of the capacity was retained after 1000 cycles.

In order to enhance the capacity and rate performance of the electrodes, Fan *et al.*[56] used 2,6-AQDS **1b** in combination with carbon nanotubes (CNTs) and a DME-based electrolyte. Reversible Q_m was up to 174 mA h g^{-1}, higher than the theoretical value. It was partially attributed to the contribution from CNTs (23 mA h g^{-1}). The authors assembled a full cell, which had pre-potassiated graphite as an anode. The cell had a Q_m of up to 87 mA h g^{-1} (per mass of AQDS) with an average discharge voltage of 1.1 V. At 500 mA g^{-1}, the capacity retention of the full cell was 33% after 2500 cycles.

Another low-molecular weight quinone with ionic substituents is tetrahydroxy-1,4-benzoquinone disodium salt **2**. Zhao *et al.*[57,58] reported that Q_m for **2** reached 190.6 mA h g^{-1} with a carbonate-based electrolyte at 25 mA g^{-1}. At 1.25 A g^{-1}, its value dropped to 45 mA h g^{-1}.[58] The capacity faded by *ca.* 50% after 50 cycles.[57,58] Although it is expected that acidic OH

Table 1 Data for organic-based cathode materials used in potassium-based batteries

#	Theoretical capacity Q_m (mA h g^{-1})	Electrode composition (weight ratio), electrode mass loading (mg cm^{-2})	Electrolyte composition; counter electrode[a]	Reversible capacity Q_m (mA h g^{-1}), current (mA g^{-1})	Potential window (V); average reduction potential (V), current (mA g^{-1})	Cycling stability: decay of reversible capacity (%), cycles, current (mA g^{-1})	1st cycle discharge/charge capacity ratio (%), current (mA g^{-1})	Ref.
1a	130	**1a** : SP : SA = 7 : 2 : 1, n.r.	0.8 M KPF_6 in EC : DEC (1 : 1 v/v); K	95, 13; 88, 26; 81, 65; 73, 130; 64, 260; 56, 390	1.4–3.0; 1.8, 13	18, 100, 13	135, 13	54
		1a : SP : SA = 7 : 2 : 1, 1.14	0.8 M KFSI in EC : DEC (1 : 1 v/v); K	97, 13; 41, 36; 28, 65; 19, 130; 12, 260; 8, 390	1.4–3.0; 1.85, 13	78, 100, 13	122, 13	55
			0.8 M KFSI in DME; K	97, 13; 97, 36; 97, 65; 97, 130; 89, 260; 84, 390	1.4–3.0; 1.75, 13	20, 1000, 390; 3, 100, 13	138, 13	
1b	130	**1b** : KB : CNT : polyacrylonitrile copolymer = 6 : 2 : 1 : 1, 3.3	1 M KPF_6 in DME; K	174, 50; 126, 100	1.0–3.0; 1.9, 50	~3, 150, 100	64, 50	56
			1 M KPF_6 in DME; KC_8 (full cell)	87, 50; 78, 100; 71, 200; 66, 300; 61, 400; 58, 500; 46, 1000	0.05–3.0; 1.1, 50	45, 250, 100; 67, 2500, 500	60, 100	
2	248	**2** : SP : PVdF = 5 : 4 : 1, 1.2	0.8 M KPF_6 in EC : DEC (1 : 1 v/v); K	168, 25; 113, 50; 91, 125; 76, 250; 56, 500; 40, 1250; 33, 2500; 27, 5000	1.0–3.0; 1.5, 50	61, 100, 25	129, 25	57
		2 : SP : PVdF = 5 : 4 : 1, 1.2	0.8 M KPF_6 in EC : DEC (1 : 1 v/v); K	190.6, 25; 152, 37; 104, 124; 80, 248; 62.5, 496; 45, 1240; 38.5, 2480; 29, 4960	1.0–3.0; 1.6, 25	53, 50, 25; 63, 2000, 2480	120, 25	58
3a	218	**3a** : SP : PVdF = 6 : 3 : 1, 1.5–2.0	1.25 M KPF_6 in DME; K	138, 200; 133, 400; 118, 1000; 113, 2000	1.0–3.2; 1.8, 100	40, 99, 200	104, 200	52
	109			68, n.r.	1.5–3.2; 2.2, n.r.	−3[b], 9, n.r.	n.r.	
			1.25 M KPF_6 in DME; **3a** (full cell)	~70, 25	0.5–2.0; 1.05, 25	45, 9, 25	39, 25	
3b	250	**3b** : SP : PVdF = 7 : 2 : 1, n.r.	1 M KFSI in DME; NaK alloy (Na : K = 33.7 : 66.3 w/w) in carbon paper	150, 50; 118, 125; 95, 250; 76, 500; 52, 1250	1.0–3.0; 1.6, 125	26, 100, 125	101, 125	59
4	246	**4** : SP : PVdF = 6 : 3 : 1, 1.5–2.0	1.25 M KPF_6 in DME; K	116, n.r. 134, n.r.	0.8–3.0; 1.3, n.r. 0.8–2.0; 1.3, n.r.	15, 10, n.r. 7, 10, n.r.		52
5	556	**5** : SP : PVdF = 5 : 4 : 1, ~0.4	1 M KTFSI in DME : DOL (1 : 1 v/v)	332, 44; ~110, 440	1.1–2.8 or 1.1–3.1; 1.6, 44	51, 50, 44; ~55, 500, 440	n.r.	60
6	343	**6** : SP : PAI = 4 : 5 : 1, n.r.	n.r.	253, 258	1.2–3.3; 1.85, 258	n.r.	111, 258	61
7	441	**7** : AB : PTFE = 7 : 2 : 1, n.r.	2.5 M KTFSI in PC	139, 40	1.3–4.3; 2.8, 40	38, 10, 40	67, 40	62
			1 M KFSI in $Pyr_{13}FSI$	231, 40	1.3–4.3; 2.3, 40	64, 1, 40	101, 40	
8	300	**8** : SP : CMC = 6 : 3 : 1[c], ~2	1 M KPF_6 in EC : PC (1 : 1 v/v); K	244, 20; 222, 50; 185, 100; 164, 200; 139, 500; 125, 1000	2.0–4.1; 2.75, 50	15, 40, 50	106, 50	63
9	137	**9** : SP : PVdF = 7 : 2 : 1, 1.4	0.5 M KPF_6 in EC : DEC (1 : 1 v/v); K	132, 10; 92, 100; 88, 200; 73, 500	1.5–3.5; 2.4, 10	35, 200, 50	97, 10	64
		9 : SP : PVdF = 7 : 2 : 1, 3.3–3.7	0.8 M KPF_6 in EC : DEC (1 : 1 v/v); K	117, 20; 97, 50; 77, 100; 56, 200	1.2–3.2; 2.4, 100	28, 244, 10	106, 20	65
		9 : SP : PVdF = 6 : 2 : 2, 1.2–1.4	Poly(propylene carbonate) + cellulose + KFSI (solid electrolyte); K	118, 10; 109, 20; 88, 50; 79, 100	1.5–3.5; 2.3, 10	16, 40, 20	103, 10	66
		9 : CB : CMC = 8 : 1 : 1, 1.2	3 M KFSI in DME; K	126, 20; 125, 50; 122, 100; 117, 200; 109, 500; 84, 1000; 51, 2000; 18, 5000	1.5–3.5; n.r.	47, 200, 1000	n.r.	67

Table 1 (*Contd.*)

#	Theoretical capacity Q_m (mA h g^{-1})	Electrode composition (weight ratio), electrode mass loading (mg cm^{-2})	Electrolyte composition; counter electrode[a]	Reversible capacity Q_m (mA h g^{-1}), current (mA g^{-1})	Potential window (V); average reduction potential (V), current (mA g^{-1})	Cycling stability: decay of reversible capacity (%), cycles, current (mA g^{-1})	1st cycle discharge/charge capacity ratio (%), current (mA g^{-1})	Ref.
		9[d] : CB : CMC = 8 : 1 : 1, 6.9	3 M KFSI in DME; K	124, 20; 125, 50; 123, 100; 122, 200; 120, 500; 119, 1000; 115, 2000; 99, 4000; 84, 5000	1.5–3.5; 2.4, 20	13, 1000, 1000; 2, 140, 100	102, 20	
		9[d] : CB : CMC = 8 : 1 : 1, n.r.	3 M KFSI in DME; pre-potassiated soft carbon (full cell)	116, 50; 109, 100; 94, 200; 80, 400; 70, 600; 63, 800; 56, 1000	0.8–3.2; 1.65, 50	35, 3000, 600	77, 50	
		9[d] : CB : CMC = 8 : 1 : 1, 1.16	1.5 M KPF_6 in DME; K	96, 100	1.5–3.5; 2.4, 100	56, 140, 100	n.r.	
		9[d] : CB : CMC = 8 : 1 : 1, 0.92	0.8 M KPF_6 in EC : EMC (1 : 1 v/v); K	104, 100	1.5–3.5; 2.3, 100	73, 140, 100	n.r.	
		9 : CMC = 95 : 5, 19.5	3 M KFSI in DME; K	101,	1.5–3.5; 2.5, 20	~0, 550, 20	n.r.	
		9 : SP : PVdF = 7 : 2 : 1, ~2.3	5 M KFSI in DME; K	140, 51[e]; 132, 101[e]; 122, 201[e]; 106, 503[e]; 94, 1004[e]; 74, 2008[e]; 40, 5022[e]; 21, 10 046[e]; 4, 20 092[e];	1.2–3.2; 2.3, 51[e]	40, 1000, 302[e]	111, 51[e]	68
10	137	**10** : KB : polyacrylonitrile copolymer (La133) = 6 : 3 : 1, 3.3	5 M KFSI in EC : DMC (1 : 1 v/v); K	137, 500; 137, 1000; 133, 2000; 128, 3000; 122, 4000; 110, 5000; 80, 10 000	1.4–3.8; 2.25, 50	~0, 100, 100; 10, 600, 4000	99, 100	69
			5 M KFSI in EC : DMC (1 : 1 v/v); KC_8 (full cell)	126, 50; 107, 100; 92, 200; 85, 300; 80, 400	1.1–3.4; 2.0, 50	47, 500, 500	102, 50	
11	200	**11** : KB : polyacrylonitrile copolymer (La133) = 6 : 3 : 1, >5	1 M KPF_6 in DME; K	220, 100; 218, 500; 209, 1000; 200, 2000; 192, 3000; 184, 4000; 180, 5000; 163, 10 000; 133, 20 000	1.0–3.8; 2.0, 100	27, 900, 3000	69, 100	70
			1 M KPF_6 + 0.05 M LiTFSI in DME; K	219, 100	1.0–3.8; 2.0, 100	4, 50, 100	81, 100	
			1 M KPF_6 in DME; pre-potassiated K_2TP (full cell)	213, 100; 201, 200; 182, 300; 170, 500; 155, 1000; 142, 2000	0.2–3.2; 1.4, 100	51, 10 000, 3000; 68, 30 000, 3000	88, 100	
12	187	**12** : AB : PVdF = 5 : 4 : 1, ~1.0	0.8 M KPF_6 in EC : PC (1 : 1 v/v); K	181, 200; 129, 300; 118, 500; 104, 1000	1.7–4.5; 2.7, 100	13, 300, 300	17, 200	71
			0.8 M KPF_6 in EC : PC (1 : 1 v/v); graphene (full cell)	181, 200; 129, 300; 118, 500; 104, 1000	1.7–4.5; 2.7, 100	13, 300, 300	17, 200	
				60, 100	0.01–3.8; 2.0, 100	16, 700, 100	36, 100	
			0.8 M KPF_6 in DME; Bi (full cell)	123, 100; 64, 200	0.01–4.0; 2.15, 200	29, 170, 100	53, 100	
P1	225	**P1** : SP : PVdF = 7 : 2 : 1, ~2.9	0.5 M KTFSI in DME : DOL (1 : 1 v/v); K	257, 100	0.01–4.0; 1.3, 200	39, 30, 100	54, 100	72
				190, 20; 106, 200	1.5–3.4; 1.9, 20	25, 50, 20; 77, 200, 200	111, 20	
			0.8 M KPF_6 in EC : DMC; K	138, 20	1.5–3.4; 2.0, 20	40, 2, 20	155, 20	
P2	227	**P2** : KB : PVdF = 6 : 3 : 1, ~3.3	1 M KTFSI in DME : DOL (1 : 1 v/v)	189, 25; 147, 50; 127, 100; 119, 250; 108, 500	1.2–3.2; 1.8, 50	45, 60, 50	107, 50	73
P3	187	**P3** : KB : PVdF = 6 : 3 : 1, ~3.3		184, 50; 177, 100; 168, 250; 154, 500	1.2–3.2; 2.0, 50	26, 70, 50; 61, 250, 250	103, 50	

Table 1 (*Contd.*)

#	Theoretical capacity Q_m (mA h g^{-1})	Electrode composition (weight ratio), electrode mass loading (mg cm^{-2})	Electrolyte composition; counter electrode[a]	Reversible capacity Q_m (mA h g^{-1}), current (mA g^{-1})	Potential window (V); average reduction potential (V), current (mA g^{-1})	Cycling stability: decay of reversible capacity (%), cycles, current (mA g^{-1})	1st cycle discharge/charge capacity ratio (%), current (mA g^{-1})	Ref.
P4	229	**P4** : KB : PVdF = 6 : 3 : 1, ~3.3		163, 25; 155, 50; 132, 100; 115, 250; 107, 500	1.2–3.2; 1.75, 50	9, 200, 250; 9.5, 60, 50	125, 50	
P5	291	**P5** : SP : CMC = 5 : 4 : 1, 1–2	1 M KPF_6 in DME; K	256, 100; 238, 500; 232, 1000; 214, 2000; 190, 5000; 169, 10 000	0.8–3.2; 1.65, 100	25, 3000, 5000	85, 100	74
			1 M KPF_6 in DME; K_2TP (full cell with pre-potassiated cathode)	253, 100	0.1–3.2; 1.4, 100	34, 100, 100	97, 100	
P6	138	**P6** : SP : PVdF = 7 : 2 : 1, ~2.3	5 M KTFSI in DME; K	141, 51[e]; 139, 102[e]; 138, 203[e]; 127, 508[e]; 109, 1015[e]; 88, 2029[e]; 62, 5074[e]; 31, 10 149[e]; 19, 20 299[e]	1.2–3.2; 2.25, 51[e]	25, 1000, 305[e]; ~0, 1000, 1015[e]	108, 51[e]	68
			5 M KTFSI in DME; pre-potassiated K_2TP (full cell)	129, 50; 121, 100; 110, 200; 97, 500; 86, 1000	0.5–2.6; 1.55, 50	29.7, 350, 300	116, 50	
P7	129	**P7** : SP : PVdF = 7 : 2 : 1, ~2.3	5 M KTFSI in DME; K	118, 48[e]; 106, 95[e]; 101, 189[e]; 97, 474[e]; 93, 946[e]; 91, 1892[e]; 78, 4732[e]; 66, 9466[e]; 53, 18 931[e]	1.2–3.2; 2.05, 48[e]	6, 1000, 284; ~0, 1000, 946[e]	130, 48[e]	
			5 M KTFSI in DME; pre-potassiated K_2TP (full cell)	118, 50; 107, 100; 100, 200; 91, 500; 83, 1000	0.5–2.6; 1.45, 50	36.9, 350, 300	127, 50	
P8	125	**P8** : SP : PVdF = 7 : 2 : 1, ~2.3	5 M KTFSI in DME; K	123, 46[e]; 111, 92[e]; 104, 183[e]; 90, 458[e]; 81, 915[e]; 64, 1831[e]; 39, 4578[e]; 21, 9157[e]; 4, 18 314[e]	1.2–3.2; 2.0, 46[e]	22, 1000, 275[e]	122, 46[e]	
P9	121	**P9** : SP : PVdF = 7 : 2 : 1, ~2.3	5 M KTFSI in DME; K	115, 45[e]; 106, 89[e]; 93, 177[e]; 76, 444[e]; 58, 886[e]; 42, 1773[e]; 10, 4433[e]; 2, 8868[e]; 1, 17 736[e]	1.2–3.2; 2.05, 45[e]	−16, 1000, 267[e]	118, 45[e]	
P10	183	**P10**@graphene : CB : CMC = 8 : 1 : 1 (**P10** : graphene ~ 21 : 4), ~1.5	KFSI : DME, 1 : 5 molar ratio; K	142, 100; 130, 200; 124, 500	1.4–3.5; 2.15, 100	−8, 500, 100	96, 100	75
			KFSI : DME, 1 : 5 molar ratio; pre-potassiated soft carbon (full cell)	71, 50	0.5–2.5; 1.05, 50	47, 80, 50	108, 50	
P11	158	**P11** : SP : PVdF = 6 : 3 : 1, n.r.	0.8 M KPF_6 in EC : DEC (1 : 1 v/v); K	158, 10; 125, 20; 115, 50; 108, 100; 102, 200; 93, 500; 74, 1000; 47, 2000	1.5–3.5; 2.2, 50	44, 200, 50	96, 50	76
P12	228	**P12** : SP : PVdF = 6 : 3 : 1, n.r.		239, 10; 147, 20; 133, 50; 123, 100; 108, 200; 97, 500; 82, 1000; 63, 2000	1.5–3.5; 2.0, 50	78, 200, 50	119, 50	
P13	146	**P13** : SP : PVdF = 6 : 3 : 1, n.r.		164, 10; 101, 20; 93, 50; 89, 100; 87, 200; 83, 500; 80, 1000; 72, 2000	1.5–3.5; 2.25, 50	40, 200, 50; 26, 1000, 1000	104, 50	
P14	422	**P14** : SP : PVdF = 4 : 5 : 1, ~1.2	1 M KPF_6 in DME; K	245, 50; 220, 100; 215, 200; 206, 500; 198, 1000; 189, 2000; 176, 5000; 169, 10 000	0.9–3.4; 1.6, 50	-3^b, 100, 500; -8^b, 4600, 10 000	120, 50	77

Table 1 (*Contd.*)

#	Theoretical capacity Q_m (mA h g^{-1})	Electrode composition (weight ratio), electrode mass loading (mg cm^{-2})	Electrolyte composition; counter electrode[a]	Reversible capacity Q_m (mA h g^{-1}), current (mA g^{-1})	Potential window (V); average reduction potential (V), current (mA g^{-1})	Cycling stability: decay of reversible capacity (%), cycles, current (mA g^{-1})	1st cycle discharge/charge capacity ratio (%), current (mA g^{-1})	Ref.
		P14 : SP : PVdF = 6 : 3 : 1, ~1.2		213, 50; 203, 100; 197, 200; 186, 500; 176, 1000; 162, 2000; 143, 5000	0.9–3.4; 1.6, 50	−3[b], 10, 50	98, 50	
		P14 : SP : PVdF = 2 : 2 : 1, ~1.8–2.4	~1.5 M KPF_6 in DME; NaK alloy (Na : K = 15 : 85 w/w) in carbon paper	185, 200; 166, 500; 158, 1000; 152, 2000; 142, 5000; 133, 10 000; 122, 20 000; 97, 50 000	1.1–3.6; 1.8, 200	11, 10 000, 10 000	n.r.	78
P15	294	**P15** : CB : PTFE = 7 : 2 : 1, 4.3	PMMA-based polymer-gel electrolyte; K	138, 10; 134, 20; 127, 50; 116, 100; 95, 200	2.0–4.0; 3.1, 10	2, 100, 50	99, 50	79
			0.8 M KPF_6 in EC : DEC : FEC (45 : 45 : 10 v/v/v); K	138, 10; 127, 20; 116, 50; 108, 100; 64, 200	2.0–4.0; 3.1, 10	20, 100, 50	92, 50	
P16	111	**P16** : AB : CMC = 8 : 1 : 1, ~1.5	0.8 M KPF_6 in EC : DEC (1 : 1 v/v); K	98, 100	2.0–4.0; 3.5, 100	28, 60, 100	43, 100	80
			0.8 M KPF_6 in EC : DEC (1 : 1 v/v); graphite (full cell)	60, 50; 40, 100; 35, 150; 31, 200; 28, 250; 24, 300	1.0–4.0; 3.23, 50	11, 120, 50; 24.5, 500, 100	87, 100	
P17	209	**P17** : SP : PVdF = 5 : 4 : 1, ~2–4	0.5 M KPF_6 in EC : DEC (1 : 1 v/v); K	63, 104.5; 63, 209; 62, 2090; 48, 10 450; 46, 20 900	2.5–4.2; 3.5, 209	14, 500, 209; 37, 1000, 2090; 80, 1000, 10 450; 85, 1000, 20 900	91, 2090	81
P 18	209	**P18** : SP : PVdF = 5 : 4 : 1, ~1	2.2 M KPF_6 in diglyme; K	139, 40; 151, 100; 162, 200; 152, 500; 148, 1000; 142, 2000; 134, 5000; 121, 10 000	2.5–4.5; 3.6, 40	−6[b], 5, 40; 5, 127, 200; 9, 200, 400; 4, 200, 1000; 38, 2000, 2000	47, 40; 64, 200	82
			1 M KPF_6 in diglyme; K	120, 40; 121, 100; 119, 200; 115, 400; 106, 1000; 97, 2000; 87, 5000; 71, 10 000	2.5–4.5; n.r.	−4[b], 5, 40	n.r.	
			2 M KTFSI in diglyme; K	116, 40; 104, 100; 100, 200; 97, 500; 95, 1000; 93, 2000; 90, 5000; 86, 10 000		8, 5, 40	n.r.	
			0.5 M KPF_6 in EC : DEC (1 : 1 v/v); K	131, 40; 115, 100; 113, 200; 110, 500; 106, 1000; 100, 2000; 91, 5000; 69, 10 000		8, 5, 40	n.r.	
			1 M KPF_6 in FEC : DMC (1 : 1 v/v); K	142, 40; 138, 100; 134, 200; 128, 500; 120, 1000; 105, 2000; 72, 5000; 35, 10 000		−3[b], 5, 40	n.r.	
			1 M KPF_6 in DME; K	78, 40; 107, 100; 106, 200; 102, 500; 95, 1000; 87, 2000; 75, 5000; 54, 10 000		—	n.r.	
		P18 : SP : PVdF = 2 : 2 : 1, ~1.8–2.4	~1.5 M KPF_6 in DME; NaK alloy (Na : K = 15 : 85 w/w) in carbon paper	171, 200; 171, 500; 170, 1000; 166, 2000; 156, 5000; 143, 10 000; 126, 20 000; 65, 50 000	2.5–4.5; 3.6, 200	31, 1500, 10 000	n.r.	78

Table 1 (*Contd.*)

#	Theoretical capacity Q_m (mA h g^{-1})	Electrode composition (weight ratio), electrode mass loading (mg cm^{-2})	Electrolyte composition; counter electrode[a]	Reversible capacity Q_m (mA h g^{-1}), current (mA g^{-1})	Potential window (V); average reduction potential (V), current (mA g^{-1})	Cycling stability: decay of reversible capacity (%), cycles, current (mA g^{-1})	1st cycle discharge/charge capacity ratio (%), current (mA g^{-1})	Ref.
P19	139	**P19** : KB : CNT : LA132 = 54 : 18 : 18 : 10, ~3.3	1 M KPF_6 in PC : FEC (98 : 2 v/v); K	117, 20; 114, 50; 108, 100; 103, 200; 93, 500; 82, 1000; 82, 1000; 68, 2000	2.0–4.7; 4.0, 20	14, 100, 50; 3, 180, 100; 30, 400, 500; 45, 500, 2000	25, 20	83

[a] If not stated otherwise, the materials were tested in two-electrode cells. [b] Reversible capacity increased after cycling. [c] An additional interlayer electrode was used in cells, see text for details. [d] Annealed at 450 °C, see text for details. [e] Equivalent of 1C rate in mA g^{-1} was undefined in the reference article; 1C rate was calculated based on the theoretical capacity.

protons should undergo irreversible substitution for K^+ upon initial discharge, the irreversible capacity at the first cycle was relatively low (38 mA g^{-1} at 25 mA g^{-1}),[58] indicating that this process was somehow suppressed. It should be noted that the rate and cycle capabilities of **2** for lithium and sodium batteries were much better than for potassium cells,[57,58] suggesting that the performance of the latter can be optimized by, for example, switching to another electrolyte.

The opportunity for this optimization indirectly follows from the data for a similar compound, potassium rhodizonate **3a**, which was tested with a DME-based electrolyte.[52] The reversible Q_m for **3a** approached 138 mA h g^{-1} at 200 mA g^{-1} in a 1.0–3.2 V *vs.* K^+/K range (avg. 1.8 V), employing a two-electron reduction/oxidation. At a high current density of 2 A g^{-1}, 113 mA h g^{-1} was still observed. The capacity fading for the half-cell was 0.4% per cycle at 200 mA g^{-1}.

Since the voltage plateaus of **3a**, each corresponding to a one-electron process, had an interval of ~1 V, it was possible to build a 1 V symmetrical full cell. Its capacity, however, faded by ~50% after 9 cycles. If the potential window was widened to 0.1–3.2 V *vs.* K^+/K, the capacity of **3a** increased to 428 mA h g^{-1} in half-cells, suggesting a four-electron reversible reduction. In this mode, the average discharge potential was ~1.0 V, and the cycling stability was not studied.

While selecting the optimal potential range for oxocarbon derivatives, it is important to know that poorly reversible transformations can occur, especially at high potentials. For example, it is known that oxidation products of rhodizonates dissolve in the electrolytes, causing a rapid capacity decay.[111–113] For this reason, only four-electron reduction is considered suitable for the practical operation of rhodizonates.

For the analogs of **3a**, such as potassium croconate **4** and potassium squarate ($K_2C_4O_4$), both the discharge potentials and the capacities significantly deteriorated with shrinking of the ring size. Noteworthily, the rate performance for the potassium batteries with **3a** was superior compared to lithium and sodium cells, which was explained by facilitated K^+ diffusion within the material.

A sodium-based analog of **3a**, *i.e.* sodium rhodizonate **3b**, was tested by Goodenough *et al.*[59] with an anode based on a liquid sodium–potassium alloy (NaK). The advantage of this anode is its dendrite-free nature, making it safer compared to pristine potassium.[114] In a DME-based KFSI solution, Q_m was ~120 mA h g^{-1} at 125 mA g^{-1}, with ~50 mA h g^{-1} delivered at 1.25 A g^{-1}. The capacity retention was *ca.* 75% after 100 cycles.

The behavior of **3b**, however, greatly changed after switching the electrolyte to 1 M $NaClO_4$ in EC : DMC. It altered the charge–discharge voltage profiles, with the average discharge potential becoming higher with the Na-based electrolyte. Additionally, the capacities, rate and cycle performance also improved with the $NaClO_4$ solution. The authors showed that Na^+ were the charge carriers when the Na-based electrolyte was used, while potassium ions were acting in the case of the K-based electrolyte. As a control experiment, the NaK-based anode was changed to pure Na or K metals. The charge–discharge profiles were almost coinciding for NaK and Na with the Na-based electrolyte, as well as for NaK and K with the K-based formulation. XRD patterns of the four discharged electrodes followed the same

Table 2 Data for organic-based anode materials used in potassium-based batteries

#	Theoretical capacity (mA h g^{-1})	Electrode composition (weight ratio), electrode mass loading (mg cm^{-2})	Electrolyte composition; counter electrode[a]	Reversible capacity (mA h g^{-1}), current (mA g^{-1})[b]	Potential window (V); average demetalation potential (V), current (mA g^{-1})	Cycling stability: decay of reversible capacity (%), cycles, current (mA g^{-1})	1st cycle discharge/charge capacity ratio (%), current (mA g^{-1})	Ref.
3a	109	**3a** : SP : PVdF = 6 : 3 : 1, 1.5–2.0	1.25 M KPF_6 in DME; K	54, n.r. 450, n.r.	1.0–1.7; 1.4, n.r. 0.1–3.0; 1.5, n.r.	3, 9, n.r. 3, 1, n.r.	n.r. 116, n.r.	52
	436							
9	410	**9** : SP : PVdF = 7 : 2 : 1, 1.4	0.5 M KPF_6 in EC : DEC (1 : 1 v/v); K	413, 10	0.01–3.0; 1.65, 10	67, 35, 10	215, 10	64
	137	**9** : SP : PVdF = 7 : 2 : 1, n.r.	30 M KFSI in H_2O; AC (3 electrode cell, Hg/Hg_2Cl_2 ref.)	134, 200; 130, 500; 130, 1000; 130, 1000; 130, 2000; 125, 4000; 110, 8000	−1.1–0.1; −0.55, 200	18, 500, 2000	108, 200	84
		9 : SP : PVdF = 7 : 2 : 1, ~1.4	30 M KFSI in H_2O; KFHCF cathode (full cell)	39[f], 200; 39[f], 500; 39[f], 1000; 38[f], 2000; 37[f], 4000	−2.0 to 0.0; −1.0, 200	11, 1000, 2000	88, 200	
10	412	**10** : CB : PVdF = 7 : 2 : 1, ~1.7	1 M KPF_6 in DME; K	320, 500; 290, 1000; 246, 2000; 208, 5000	0.01–3.0; 1.5, 500	37, 100, 500; 7, 320, 5000	152, 500	85
			1 M KPF_6 in PC : EC (1 : 1 v/v); K	131, 500; 73, 1000; 47, 2000; 22, 5000	0.01–3.0; 1.9, 500	46, 100, 500	367, 500	
	137	**10** : CB : PVdF = 7 : 2 : 1, 5.2	CF_3SO_3K in H_2O (22 mol CF_3SO_3K per 1 L H_2O); AC (3 electrode cell, Ag/AgCl ref.)	125, 65; 120, 520; 114, 1300; 110, 2600	−1.3 to 0.3; −0.4, 65	23, 1000, 2600	129, 65	86
13a	221	**13a** : SP : PVdF = 6 : 3 : 1; 2–2.7	0.8 M KPF_6 in EC : DEC (1 : 1 v/v); K	100, 50	0.1–2.0; 0.75, 50	−15[c], 50, 50	323, 50	87
			1 M KPF_6 in EC : PC (1 : 1 v/v); K	177, 50	0.1–2.0; 0.8	45, 50, 50	233, 50	
			1 M KPF_6 in PC; K	215, 50	0.1–2.0; 1.1	100, 50, 50; 87, 5, 50	249, 50	
			1 M KPF_6 in DME; K	260, 50; 249, 100; 229, 200; 202, 500; 185, 1000	0.1–2.0; 0.7, 50	8, 100, 200; 8, 100, 500; 5.4, 500, 1000	131, 50	
		13a@CNT : PVdF = 9 : 1 (**13a** : CNT ~ 5.29), ~1.3	1 M KPF_6 in DME; K	250, 125; 236 (221[d]), 250; 225, 500; 218, 1250; 203, 2500; 190, 3750; 181, 5000; 165, 7500; 149, 10 000; 130, 12 500	0.2–2.0; 0.7, 125	15, 400, 1250	131, 250	88
		13a : SP : PVdF = 6 : 3 : 1, 2–2.7	1.5 M KPF_6 in DME; K	258, 100; 242, 200; 214, 500; 187, 1000; 160, 2000; 124, 5000	0.2–1.4; 0.7, 100	9.5, 100, 500	185, 500	89
		13a : SP : AB : PVdF = 5.6 : 1.4 : 2 : 1, ~2.9	1 M KFSI in EC : DMC (1 : 1 v/v); K	270 (210[d]), 11; 213, 22; 183, 44; 136, 110; 94, 220; 55, 440	0.1–2.0; 0.75, 11	40, 100, 22	217, 11	90
		13a : AB : PVdF = 6 : 3 : 1, 1.5–2.0	0.8 M KPF_6 in DME; K	59, 50; 45, 100; 31, 200; 11, 500; 4, 1000	0.1–2.0; 0.8, 50	85, 100, 200	177, 200	91
		13a@GO : AB : PVdF = 6 : 3 : 1 (**13a** : GO = 20 : 1), 1.5–2.0		288, 50; 243, 100; 198, 200; 144, 500; 109, 1000	0.1–2.0; 0.8, 50	~0, 100, 200; ~0, 400, 500; 30, 450, 1000	131, 200	
13b	323	**13b** : SP : La132 = 6 : 3 : 1, ~3.3	1 M KFSI in EC : DMC (1 : 1 v/v); K	280 (219[d]), 20; 240, 50; 193, 100; 108, 200; 56, 400	0.1–2.0; 0.75, 20	9, 150, 50	312, 20	92

Table 2 (*Contd.*)

#	Theoretical capacity (mA h g^{-1})	Electrode composition (weight ratio), electrode mass loading (mg cm^{-2})	Electrolyte composition; counter electrode[a]	Reversible capacity (mA h g^{-1}), current (mA g^{-1})[b]	Potential window (V); average demetalation potential (V), current (mA g^{-1})	Cycling stability: decay of reversible capacity (%), cycles, current (mA g^{-1})	1st cycle discharge/charge capacity ratio (%), current (mA g^{-1})	Ref.
13c	339	**13c** : AB : CMC = 6 : 3 : 1, 1.3–2.0	1 M KPF_6 in DME; K	450, 50; 271, 100; 228, 200; 201, 300; 159, 600; 131, 1000	0.2–3.0; 1.25, 50	36, 50, 100; 50, 200, 200, 20, 597, 1000	165, 50	93
13d	240	**13d** : AB : PVdF = 6 : 3 : 1, 1.7–2.7	1 M KFSI in EC : DMC (1 : 1 v/v); K	112, 60; 50, 120; 0, 240	0.005–2.0 or 0.1–2.0; 1.1, 60	59, 200, 60	556, 60	94
		13d : SP : AB : PVdF = 5.4 : 0.6 : 3 : 1, 1.7–2.7		242, 60; 66, 240; 27, 480	0.005–2.0 or 0.1–2.0; 0.95, 60	45, 200, 60	263, 60	
13e	n.r.	**13e**@CNT : SP : PVdF = 6 : 3 : 1, ~3.3	1 M KFSI in EC : DEC (1 : 1 v/v); K	234[e] (207[d]), 20; 157[e], 50; 126[e], 100; 101[e], 200; 47[e], 400	0.01–3.0; 1.1, 20	~0, 50, 50; 40, 200, 200	343, 20	95
14	220	**14** : SP : AB : PVdF = 5.6 : 1.4 : 2 : 1, ~2.9	1 M KFSI in EC : DMC (1 : 1 v/v); K	245 (185[d]), 11; 201, 22; 179, 44; 163, 110; 110, 220; 79, 440	0.1–2.0; 0.85, 11	16, 100, 22	227, 11	90
15	168	**15** : SP : CMC = 6 : 3 : 1, ~3.3	1 M KFSI in EC : DMC (1 : 1 v/v); K	144, 10; 129, 20; 105, 50; 93, 100; 76, 200; 52, 500	0.1–2.5; 0.9, 10	12, 100, 20	159, 10	96
		15@graphene : SP : CMC = 6 : 3 : 1 (**15** : graphene = 95 : 5), ~3.3		211, 10; 202, 20; 178, 50; 165, 100; 143, 200; 135, 500; 99, 1000	0.1–2.5; 0.9, 10	24, 100, 50; 58, 3000, 1000	199, 10	
16	156	**16** : SP : CMC = 6 : 3 : 1, ~3.3		132, 10; 101, 20; 74, 50; 55, 100; 40, 200; 26, 500	0.1–2.5; 1.05, 10	43, 100, 20	159, 10	
		16@graphene : SP : CMC = 6 : 3 : 1 (**16** : graphene = 95 : 5), ~3.3		229, 10; 136, 100; 117, 200; 98, 500; 66, 1000	0.1–2.5; 1.05, 10	43, 100, 50	284, 10	
17	183	**17** : SP : PVdF = 6 : 3 : 1, ~4.2	1 M KFSI in EC : DMC (1 : 1 v/v); K	206, 10; 118, 50; 88, 100; 71, 200; 55, 500	0.1–2.0; 0.8, 10	51, 200, 50	237, 10	97
		17 : SP : CNT : PVdF = 6 : 2 : 1 : 1, ~4.2	1 M KFSI in EC : DMC (1 : 1 v/v); K	250, 10; 171, 50; 131, 100; 104, 200; 76, 500	0.1–2.0; 0.8, 10	45, 300, 100; 52, 500, 500	240, 10	
18	93	**18** : SP : PVdF = 6 : 3 : 1, >3.3	1 M KFSI in EC : DMC (1 : 1 v/v); K	143, 20; 118, 50; 100, 100; 78, 200; 31, 500	0.1–2.0; 1.1, 50	46, 300, 50	321, 20	98
		18 : AB : CNT : PVdF = 6 : 2.5 : 0.5 : 1, >3.3		143, 20; 132, 50; 107, 100; 99, 200; 78, 500	0.1–2.0; 1.1, 50	26, 300, 50; 32, 2500, 500	352, 20	
19	155	**19** : CB : SA = 6 : 3 : 1, ~1.1	0.8 M KPF_6 in EC : DEC (1 : 1 v/v); K	134, 15.5; 100, 31; 95, 77.5; 86, 155; 76, 310; 69, 775; 66, 1550	0.5–3.0; 1.55, 15.5	19, 100, 15.5; 49, 1000, 310	248, 15.5	99
20	326	**20** : SP : PVdF = 8 : 1 : 1, 0.8	n.r.	260, 5; 170, 10; 115, 20; 85, 30; 65, 50	0.01–3.0; 0.9, 5	n.r.	n.r.	100
21	313.5	**21** : AB : PVdF = 6 : 3 : 1, 0.9	0.8 M KPF_6 in EC : DEC (1 : 1 v/v); K	118, 50; 87, 100; 66, 200; 40, 500; 15, 1000	0.2–2.5; 1.6, 100	54, 100, 100	185, 100	101
		21@CNT : AB : PVdF = 6 : 3 : 1 (**21** : CNT = 9 : 1), 0.9		256[e], 50; 221[e], 100; 203[e], 200; 18; 1[e], 500; 165[e], 1000	0.2–2.5; 1.6, 100	25, 100, 100	137, 100	

Table 2 (*Contd.*)

#	Theoretical capacity (mA h g^{-1})	Electrode composition (weight ratio), electrode mass loading (mg cm^{-2})	Electrolyte composition; counter electrode[a]	Reversible capacity (mA h g^{-1}), current (mA g^{-1})[b]	Potential window (V); average demetalation potential (V), current (mA g^{-1})	Cycling stability: decay of reversible capacity (%), cycles, current (mA g^{-1})	1st cycle discharge/charge capacity ratio (%), current (mA g^{-1})	Ref.
P1	225	**P1** : SP : PTFE = 7 : 2 : 1, 52.8	10 M KOH in H_2O; AC (3 electrode cell, Hg/HgO ref.)	200, 100	−1.05 to 1.0; −0.63, 100	n.r.	n.r.	102
			10 M KOH in H_2O; $Ni(OH)_2$ cathode (full cell)	200, 112.5; 195, 225; 192, 450; 190, 1125; 185, 2250; 163, 4500	From −1.45 to −0.35; −1.0, 112.5	12, 1300, 225	80.4, 225	
P10	183	**P10** : SP : PVdF = 6 : 3 : 1, 8.3–13.3	Saturated solution of KNO_3 (~3.75 M) in H_2O; AC (3 electrode cell, Hg/Hg_2Cl_2 ref.)	135, 360; 122, 900; 112, 1800; 109, 2160; 106, 2700; 103, 3240; 100, 3600; 93, 5400	From −1.0 to −0.2; −0.55, 360	24, 300, 360	137, 360	103
			Saturated solution of K_2SO_4 (~0.69 M) in H_2O; AC (3 electrode cell, Hg/Hg_2Cl_2 ref.)	139, 360; 119, 900; 106, 1800; 101, 2160; 92, 2700; 84, 3240; 80, 3600; 60, 5400	From −1.0 to −0.2; n.r.	6, 5, 360	n.r.	
			Saturated solution of KNO_3 in H_2O; FeHCF cathode (full cell)	56[f], 360; 54[f], 900; 51[f], 1800; 50[f], 2700; 48[f], 3600; 46[f], 5400; 45[f], 7200; 45[f], 7200	−2.0 to 0.0; −0.85, 360	26, 300, 360	103, 360	
P20	n.r.	**P20** : AB : SA = 5 : 3 : 2, ~1.4	0.8 M KPF_6 in EC : DEC (1 : 1 v/v); K	227, 50	0.1–3.0; 1.05, 50	1, 1, 50	426, 50	104
P21	n.r.	**P21** : AB : SA = 5 : 3 : 2, ~1.4		233, 50	0.1–3.0; 1.5, 50	40, 1, 50	535, 50	
P22	n.r.	**P22** : AB : SA = 5 : 3 : 2, ~1.4		172, 50	0.1–3.0; 1.25, 50	1, 1, 50	709, 50	
P23	280	**P23** : AB : SA = 5 : 3 : 2, ~1.4		428 (358[d]), 30; 333, 50; 242, 100; 150, 200; 104, 500	0.1–3.0; 1.8, 50	35, 500, 50	234, 50	
P24	n.r.	**P24** : AB : SA = 5 : 3 : 2, ~1.4		183, 50	0.1–3.0; 1.0, 50	0, 1, 50	483, 50	
P25	n.r.	**P25** : AB : SA = 5 : 3 : 2, ~1.4		257, 50 p	0.1–3.0; 1.65, 50	6, 1, 50	422, 50	
P26	n.r.	**P26** : AB : PVdF = 7 : 2 : 1, ~2.1	1 M KFSI in EC : DEC (1 : 1 v/v)	202, 25; 148, 50; 72, 100; 45, 200; 31, 500; 22, 1000; 13, 2000; 9, 5000	0.005–3.0; 1.5, 100	55, 500, 100	475, 100	105
		P26@CNT : AB : PVdF = 7 : 2 : 1 (**P26** : CNT = 4 : 1), ~2.1		330[e], 25; 305[e], 50; 283[e], 100; 242[e], 200; 206[e], 500; 157[e], 1000; 103[e], 2000; 67[e], 5000	0.005–3.0; 1.4, 100	17, 500, 100; 40, 4000, 1000	262, 100	
P27	58	**P27** : AB : CMC = 7 : 2 : 1, 1.4	0.8 M KPF_6 in EC : DEC (1 : 1 v/v); K	73, 50; 63, 100; 52, 200; 46, 300; 39, 500; 35, 700; 31, 1000	0.01–3.0; 1.1, 50	30, 200, 100	550, 50	106
P28	174	**P28** : AB : CMC = 7 : 2 : 1, 1.4	0.8 M KPF_6 in EC : DEC (1 : 1 v/v); K	152, 50; 135, 100; 114, 200; 99, 300; 84, 500; 72, 700; 63, 1000	0.01–3.0; 1.0, 50	27, 200, 100	379, 50	106
P29	n.r.	**P29** : AB : PVdF = 7 : 2 : 1, ~1.5	1 M KFSI in EC : DEC (1 : 1 v/v); K	450, 100; 218, 200; 145, 500; 83, 1000; 58, 2000	0.005–3.0; 1.55, 100	49, 200, 100	203, 100	107

Table 2 (*Contd.*)

#	Theoretical capacity (mA h g^{-1})	Electrode composition (weight ratio), electrode mass loading (mg cm^{-2})	Electrolyte composition; counter electrode[a]	Reversible capacity (mA h g^{-1}), current (mA g^{-1})[b]	Potential window (V); average demetalation potential (V), current (mA g^{-1})	Cycling stability: decay of reversible capacity (%), cycles, current (mA g^{-1})	1st cycle discharge/charge capacity ratio (%), current (mA g^{-1})	Ref.
P30	n.r.	**P30** : CB : CMC = 6 : 2 : 2, 1.1–2.2	1 M KFSI in EC : DEC (1 : 1 v/v); K	54, 30	0.0–3.0; 1.2, 30	~0, 80, 30	131, 30	108
P31	n.r.	**P31** : AB : CMC = 7 : 2 : 1, ~2.9	0.8 M KPF_6 in EC : DEC (1 : 1 v/v) + 5% FEC; K	450, 50; 313, 100; 227, 200; 149, 500; 104, 1000; 73, 2000; 55, 3000	0.01–3.0; 1.7, 50	−30[c], 200, 50	148, 50	109
P32	278	**P32** : SP : CMC = 6 : 3 : 1, ~1.7	1.5 M KPF_6 in DME; K	244 (220[d]), 100; 245 (222[d]), 200; 237 (217[d]), 500; 228 (210[d]), 1000; 213 (198[d]), 2000; 170 (159[d]), 5000; 110 (104[d]), 10 000	0.5–2.0; 1.4, 100	4, 200, 1000	145, 100	110
		P32 : SP : CMC = 8 : 1 : 1, ~1.6		228 (222[d]), 100; 225 (220[d]), 200; 210 (205[d]), 500; 186 (182[d]), 1000	0.5–2.0; 1.4, 100	n.r.	n.r.	
		P32 : SP : CMC = 8 : 1 : 1, ~5.0		226, 50; 212 (207[d]), 100; 193 (188[d]), 200; 162 (157[d]), 500; 122 (118[d]), 1000	0.5–2.0; n.r.			
		P32 : SP : CMC = 8 : 1 : 1, ~15.2		224, 50; 160 (154[d]), 100				

[a] If not stated otherwise, the materials were tested in two-electrode cells. [b] If not stated otherwise, the capacity was calculated per organic material mass unit, and the contribution to the capacity from the carbon additives was not subtracted. [c] Reversible capacity increased after cycling. [d] The capacity was calculated per organic material mass unit, and the contribution to the capacity from the carbon additive was subtracted. [e] The capacity was calculated per material@CNT composite mass unit, and the contribution to the capacity from carbon black was not subtracted. [f] The capacity was calculated per combined mass of cathode and anode.

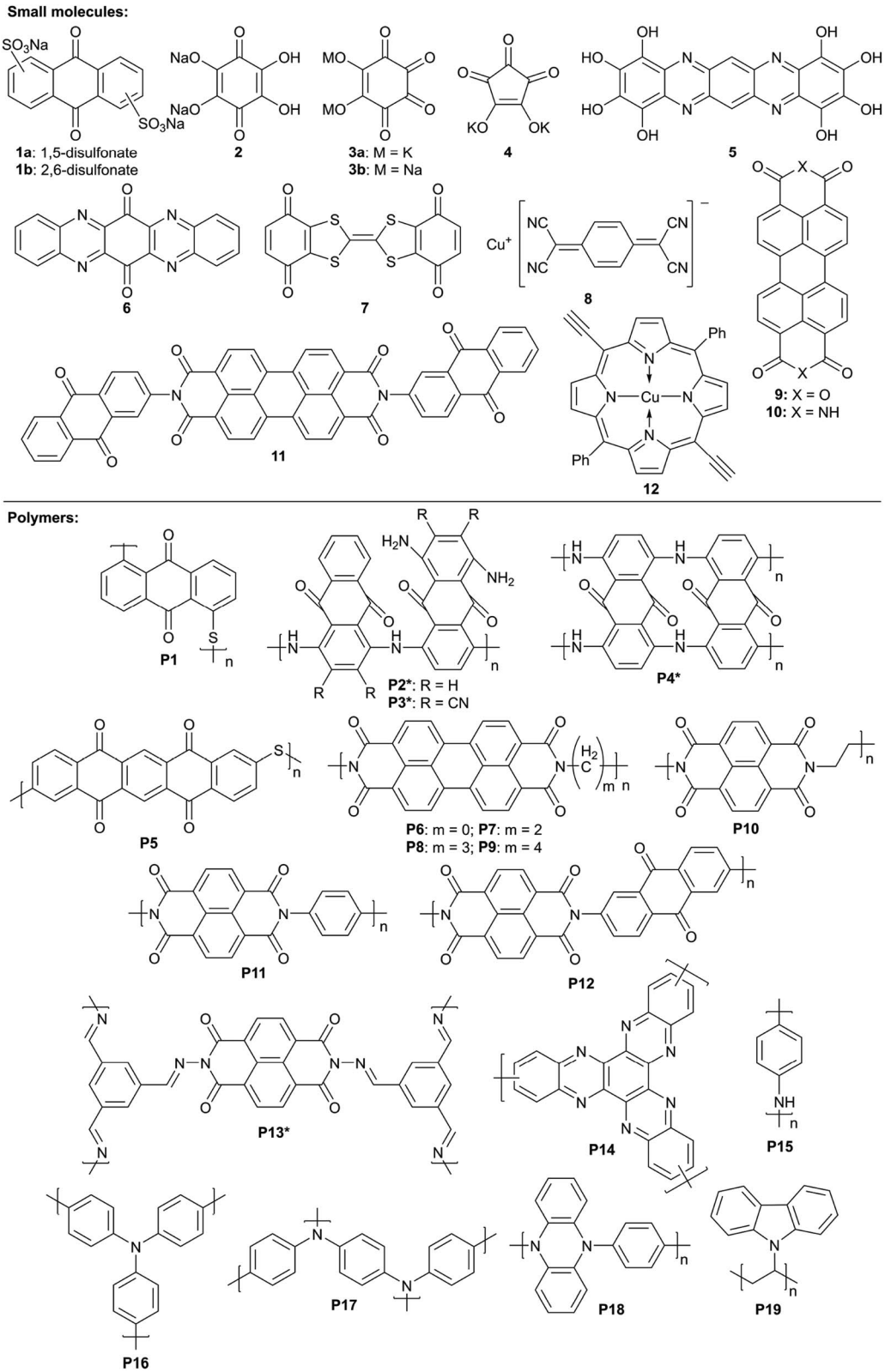

Fig. 1 Structures of organic-based cathode materials for potassium batteries. The asterisk (*) means that the actual structure of the material might be different from the depicted structure, which was proposed but not confirmed by the authors.

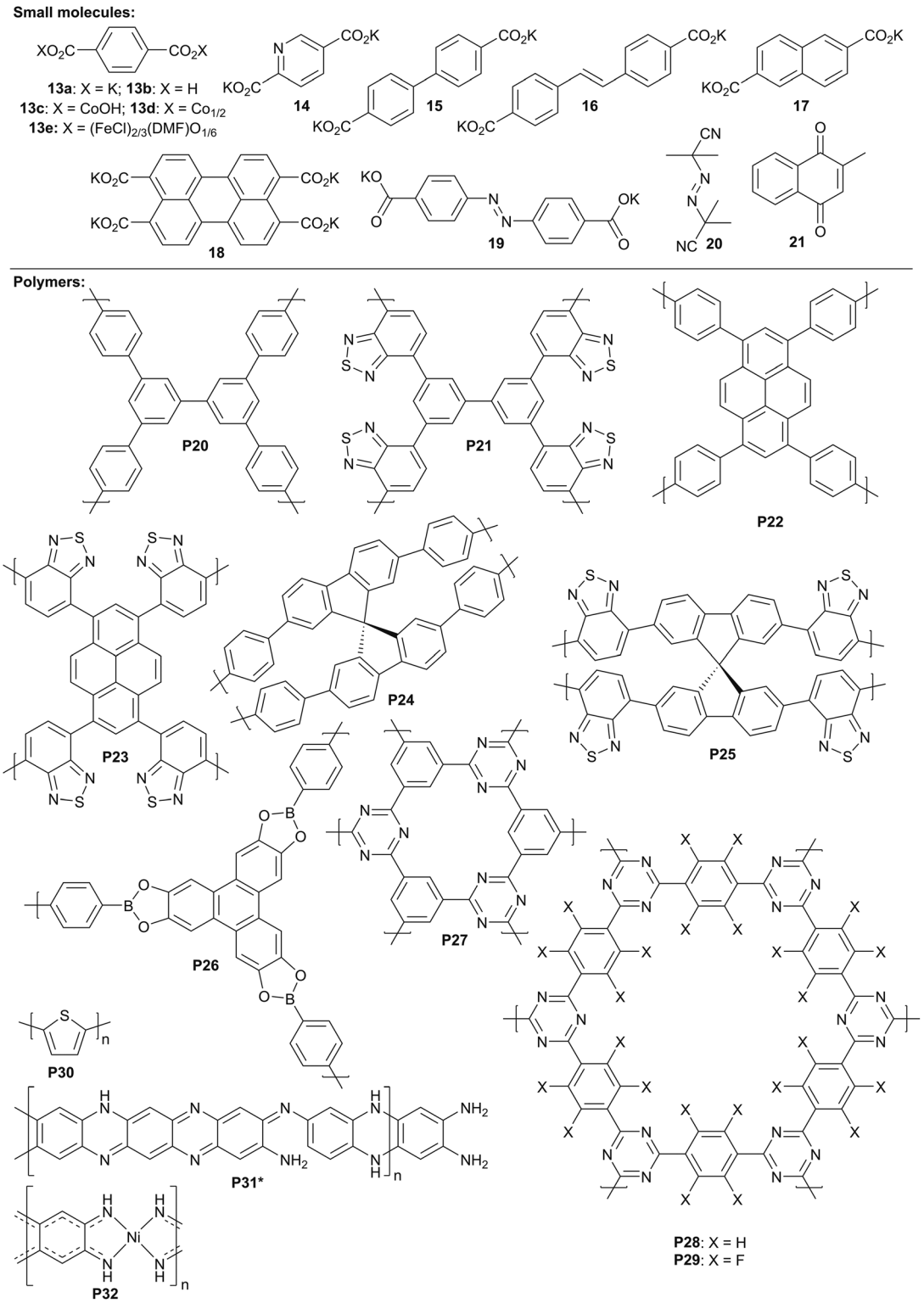

Fig. 2 Structures of organic-based anode materials for potassium batteries. Asterisk (*) means that the actual structure of the material might be different from the depicted structure, which was proposed but not confirmed by the authors.

trend. There was no evidence that the mechanisms changed upon prolonged cycling. This phenomenon was explained by the nature of the SEI layers covering the NaK-based anode, which were permeable only by one type of ion in each case.

Another group of low-molecular quinones for potassium batteries is represented by derivatives of tetraazapentacene. Troshin *et al.*[60] proposed **5**, which was synthesized as a tetrahydrate from tetrahydroxy-1,4-benzoquinone and 1,2,4,5-

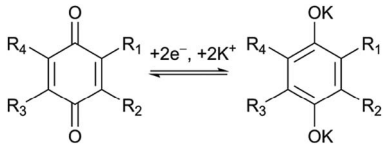

Scheme 1 Charge–discharge mechanism for 1,4-quinones.

benzenetetramine. It was suggested that all OH groups might be oxidized to carbonyls, and that pyrazine units might reversibly accept two electrons, resulting in a large theoretical Q_m of 556 mA h g^{-1}. In the potential range of 1.1–2.8 V *vs.* K^+/K, the experimental capacity approached ~330 mA h g^{-1} at the second cycle at 44 mA g^{-1}, which faded to 162 mA h g^{-1} after 50 cycles due to the material dissolution in the electrolyte. At a higher current density of 440 mA h g^{-1}, ~45% of the capacity could be retained after 500 cycles.

Another tetraazapentacene derivative **6** with two carbonyl groups was investigated by Fu *et al.*[61] At the first cycle, the reversible Q_m approached 253 mA h g^{-1} at ~1C rate (current density was 258 mA g^{-1}) in a 1.2–3.3 V *vs.* K range. No studies on rate and cycle performance were carried out for these cells.

Other cathode materials (structures **7** and **8**), which are based on quinone or quinoid small molecules, while incorporating other redox-active structural units, are discussed in Section 2.2.

Polymers. Using polymeric analogs of small molecules might be an effective strategy to circumvent the solubility issue of organic redox-active materials. The first polymeric cathode material for potassium batteries was poly(anthraquinonyl sulfide) (PAQS, **P1**).[72] With an ether-based electrolyte (0.5 M KTFSI in DME : DOL) it showed a reversible Q_m of 200 mA h g^{-1} at 20 mA g^{-1}. A capacity fading of 25% was observed after 50 cycles, while the cyclability with a carbonate-based electrolyte was inferior.

Jiang *et al.*[73] proposed a series of polymers **P2**, **P3** and **P4**, which were synthesized by oxidative polymerization of diaminoanthraquinones. The materials were probed only by FTIR spectroscopy, gel-permeation chromatography, SEM and XRD, so no detailed information about the actual molecular structures was available, although the presence of quinone units was confirmed. The reversible capacities reached with these materials were 160–185 mA h g^{-1}. Among the polymers, **P4** demonstrated the best cycling stability (9% fade after 200 cycles at 250 mA g^{-1}), apparently owing to its limited solubility. **P3**, which contained electron-withdrawing nitrile groups, showed an enhanced average discharge potential of 2.0 V *vs.* K^+/K, while the other two materials showed values of ~1.8 V.

Wang *et al.*[74] showed that poly(pentacenetetraone sulfide) (PPTS, **P5**) might be suitable for fast and stable potassium batteries. The material exhibited a high reversible capacity of ~260 mA h g^{-1} at 0.1 A g^{-1} with the average discharge potential of ~1.65 V. At 10 A g^{-1}, Q_m approached ~160 mA h g^{-1}. In half-cells, a capacity of ~190 mA h g^{-1} was retained after 3000 cycles at 5 A g^{-1}. The authors constructed an all-organic full cell with potassium terephthalate as the anode material. The cathode was electrochemically pre-potassiated. The cell delivered a capacity of 254 mA h g^{-1} at 0.1 A g^{-1} (per PPTS mass unit) and showed decent capacity retention of 66% after 100 cycles. Average voltage after 100 cycles was 1.4 V, providing the energy density of 80.5 W h kg^{-1} based on the total mass of the electrodes.

2.2 Other structures with quinoid moieties

The key disadvantage of quinones in potassium batteries is their low reduction potentials (typically 1.6–2.0 V *vs.* K, see details in Table 1 and Section 2.7). To enhance the voltage, additional functional units that enable p-doping, *i.e.* material oxidation that leads to an organic-based cation (or radical-cation) formation, might be added.

One example of such structure tuning is Q-TTF-Q **7**.[62] The molecule contains tetrathiafulvalene units, which can be reversibly oxidized at 3–4 V *vs.* Li^+/Li.[115] The average discharge voltage of **7** in K-based half cells was 2.3–2.8 V, with the capacity of ~140–230 mA h g^{-1} (depending on the electrolyte composition). However, the cycling stability was inferior, which was likely associated with the small molecule dissolution.

Another compound with p-doping capabilities is CuTCNQ **8**, proposed by Li *et al.*[63] Cu^+ and $TCNQ^-$ can be oxidized to Cu^{2+} and $TCNQ^0$, respectively; additionally, $TCNQ^-$ species can be reduced to $TCNQ^{2-}$. Overall, p-doping and n-doping (*i.e.* material reduction that leads to an organic-based anion or radical-anion formation) mechanisms provided a Q_m of 244 mA h g^{-1} at 20 mA g^{-1} and the average potential of 2.75 V *vs.* K^+/K. A decent capacity of 125 mA h g^{-1} was delivered at 1 A g^{-1}. Notably, $TCNQ^{x-}$ species formed during charge/discharge were soluble, which could be detrimental to the cycling stability.[116] To address this issue, the authors used an additional carbon interlayer, which decreased shuttling of the soluble species to the anode. By using this strategy, the capacity of 170 mA h g^{-1} could be retained after 50 cycles at 50 mA g^{-1}.

2.3 Aromatic anhydrides and imides

When used as cathode materials, anhydrides and imides of tetracarboxylic aromatic acids undergo two-electron reversible reduction, as depicted in Scheme 2.[50] The reduction of the remaining carbonyls occurs at low voltages; it is generally considered irreversible,[10,117] although some data on using these structures as anode materials[85] indicate the opposite (see Section 3.3).

Small molecules. Perylenetetracarboxylic dianhydride (PTCDA **9**) was relatively widely studied in potassium batteries.[64–67] It was first proposed for K-based cells by Hu *et al.*,[64] who tested it with a carbonate-based electrolyte. The material delivered a Q_m of 130 mA h g^{-1} at 10 mA g^{-1} with an average discharge potential of 2.4 V, while 66% of that capacity was retained after 200 cycles. At 500 mA g^{-1}, the capacity dropped to 73 mA h g^{-1}.

Reported strategies for improving the performance of PTCDA include optimization of the electrolyte composition and altering the material structure/morphology. Feng *et al.*[66] reported that a poly(propylene carbonate)-based solid-state

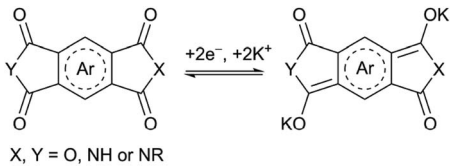

Scheme 2 Charge–discharge mechanism for aromatic anhydrides and imides.

electrolyte improved the cycling stability compared to a carbonate-based solution. However, the rate capability was modest (79 mA h g^{-1} at 100 mA g^{-1}), which is likely associated with a relatively low conductivity of the electrolyte (1.36×10^{-5} S cm^{-1} at 20 °C).

Lu *et al.*[67] used a combination of the electrolyte tuning and high-temperature treatment of PTCDA to achieve superior rate and cycling capabilities. PTCDA was annealed at 450 °C, which caused its transformation from β- to α-phase,[118] accompanied by a significant increase of electrical conductivity from $<10^{-10}$ to 5.32×10^{-6} S m^{-1}. With 0.8 M KPF_6 in EC : DMC and 1.5 M KPF_6 in DME solutions, the capacity of PTCDA faded rapidly. However, superior stability, *i.e.* 86.7% retention after 1000 cycles at 1 A g^{-1}, was achieved with 3 M KFSI in DME. This improvement was attributed to suppressed solubility of the material in the concentrated electrolyte. However, it should be noted that pristine PTCDA delivered inferior capacities and cycling stabilities even in 3 M KFSI in DME, stressing the importance of the heat treatment.

With the optimized electrolyte, annealed PTCDA showed a decent rate performance (84 mA h g^{-1} at 5 A g^{-1}). Moreover, the electrode mass loading could be increased to 19.5 mg cm^{-2}, pushing the areal capacity to ~2 mA h cm^{-2}, which is a record for all potassium-based cells reported to date (see Section 2.7). The capacity of the electrode with ultrahigh loading showed virtually no decay over 550 cycles at 20 mA g^{-1} (8 months of cycling). The authors assembled full cells using pre-potassiated soft carbon as an anode. In the full cell, the material showed up to 116 mA h g^{-1} at 50 mA g^{-1} and 56 mA h g^{-1} at 1 A g^{-1}. In addition, long cycling stability over 3000 cycles with 65% capacity retention was demonstrated.

Imide-functionalized small molecules are represented by 3,4,9,10-perylene-tetracarboxylic diimide (PTCDI **10**), recently proposed by Fan *et al.*[69] It has lower solubility compared to PTCDA,[119] which should have improved its cycling stability. Nevertheless, with 1 M and 3 M KFSI solutions in EC : DMC, rapid capacity fading associated with the material dissolution was observed. The cathode dissolution was suppressed by using 5 M KFSI in EC : DMC, which ensured ~0% capacity decay over 100 cycles at 100 mA g^{-1} and ~90% retention after 600 cycles at 4 A g^{-1}. The reported Q_m at 100 mA g^{-1} was 157 mA h g^{-1}, which is higher than the theoretical value of 137 mA h g^{-1}; the additional capacity (~27 mA h g^{-1}) originated from the carbon additive. Impressive capacities of 137 and 80 mA h g^{-1} were observed at 1 and 10 A g^{-1}, respectively. The rate performance of PTCDI was reported to be superior compared to PTCDA under the same conditions. PTCDI-based full cells, which had pre-potassiated graphite as the anode, delivered a Q_m of 140 and 80 mA h g^{-1} at 50 and 500 mA g^{-1}, respectively. The output voltage was 2 V and ~50% of the capacity retained after 500 cycles at 500 mA g^{-1}.

Recently, Fan and co-authors[70] proposed a PTCDI derivative with anthraquinone moieties (PTCDI-DAQ **11**). This compound has lower solubility than PTCDI due to the increased molecular weight, as well as higher theoretical capacity of 200 mA h g^{-1}. The observed Q_m was up to 220 mA h g^{-1}, again higher than the theoretical value. A decent capacity retention of 73% was demonstrated in the electrolyte with relatively low salt concentration (1 M KPF_6 in DME). Moreover, a remarkable capacity of 137 mA h g^{-1} was obtained at 20 A g^{-1}. A full cell with pre-potassiated terephthalate (K_4TP) anode had a high energy density of 295 W h kg^{-1} (213 mA h g^{-1} × 1.38 V, calculated per cathode mass), excellent rate capabilities (94 mA h g^{-1} at 10 A g^{-1}), and cycling stability (49% and 32% retention after 10 000 and 30 000 cycles, respectively).

Polymers. Lee *et al.*[68] investigated a series of PTCDA-based polyimides **P6–P9**, which were derived from hydrazine or aliphatic diamines. With 5 M KTFSI in DME as the electrolyte, all materials showed better cyclability than pristine PTCDA, which was attributed to their limited solubility. The polymers with the shortest linkers (**P6** and **P7**) showed virtually no signs of capacity decay after 1000 cycles at 7.35C, as well as improved rate capability. Particularly, **P7** had an energy density of 113 W h kg^{-1} when discharged at 147C rate (<10 s). The authors constructed full cells using **P6** or **P7** and pre-potassiated potassium terephthalate. These organic batteries had the energy density of up to 204 W h kg^{-1} per cathode active material mass, good rate capability, and up to 70% capacity retention after 300 cycles.

Lu *et al.*[75] tested polyimide **P10** and its composites with graphene or CNTs. Without the mentioned carbon additives, Q_m was very low. With CNTs, the capacity improved, but the cycling stability was surprisingly poor. With graphene, a stable Q_m of ~140 mA h g^{-1} was reached, being nearly constant in the 50–500 mA g^{-1} current density range. A full cell with pre-potassiated soft carbon showed a reversible capacity of ~70 mA h g^{-1} at 50 mA g^{-1} (per **P10** mass) and delivered 51 mA h g^{-1} after 80 cycles.

Ning *et al.*[76] studied a series of NTCDA-based polymeric imides **P11–P13**. Linear polymer **P12**, which had additional active anthraquinone units, showed the highest initial reversible capacity of ~240 mA h g^{-1} at 10 mA g^{-1}, which, however, faded to ~150 mA h g^{-1} already after 10 cycles. Another linear polymer **P11**, which had phenylene units instead of quinone moieties, had slightly better cyclability but delivered lower capacities (up to ~150 mA h g^{-1}). **P13**, which supposedly had a two-dimensional backbone, had a slightly improved cycling stability compared to **P11**, with 40% capacity fading after 200 cycles at 50 mA g^{-1} and 26% decay after 1000 cycles 1 A g^{-1}. It also had the best rate performance, delivering a Q_m of 72 mA h g^{-1} at 2 A g^{-1}. It should be noted that the elemental composition of **P13** significantly differs from what is expected for the structure proposed by the authors, suggesting that it should have a high defect concentration and probably can be hydrated.

2.4 Hexaazatriphenylene-based polymers

Compounds derived from hexaazatriphenylene (HAT) might reversibly accept up to six electrons per HAT unit and have excellent cycling capabilities. They might withstand 10 000–50 000 cycles with small capacity fading.[120,121] Kapaev *et al.*[77] showed that HAT-based polymer **P14** delivered a Q_m of up to 245 mA h g^{-1} at 50 mA g^{-1} in a 0.9–3.4 V *vs.* K potential range. Interestingly, the reversible capacity continuously increased upon cycling at 10 A g^{-1} from 150 to 169 mA h g^{-1} after 4600 cycles. This slow activation, of which the reasons are yet unknown, makes **P14** the most stable among all reported cathode materials for non-aqueous K-based batteries. After 4600 cycles, the cells short-circuited due to dendrite formation at the potassium anode.

To circumvent the dendrite issue, potassium was replaced by a liquid NaK-based anode.[78] Capacity fading of **P14** started after ~6000 cycles, leading to an overall 89% capacity retention after 10 000 cycles at 10 A g^{-1}. Additionally, even faster charge–discharge was demonstrated, with Q_m reaching ~100 mA h g^{-1} at 50 A g^{-1} (discharge in ~7 s).

2.5 Aromatic amines

Aromatic polymeric amines might be reversibly oxidized according to Scheme 3. In this case, anions of the supporting salt (typically KPF_6) balance the positive charge at the backbone. Cells that undergo these p-doping mechanisms are denoted as dual-ion batteries, in contrast to classic rocking-chair systems, where only metal ions act as charge carriers.[10] The main advantage of aromatic amines compared to n-type organic-based cathode materials is their high discharge potentials of >3 V *vs.* K^+/K.

One of the most popular aromatic polyamines is polyaniline (PANI, **P15**),[122] which is easy to synthesize and has a large theoretical Q_m of 294 mA h g^{-1}. Goodenough *et al.*[79] used PANI with a poly(methyl methacrylate)-based gel electrolyte to suppress the dendrite formation. The gel electrolyte enabled better rate and cycle performance compared to a liquid carbonate-based electrolyte, owing to the suppression of parasitic processes at the electrodes. Particularly, a Q_m of 138 mA h g^{-1} was delivered at 10 mA g^{-1} in a 2.0–4.0 V *vs.* K^+/K range, and 95 mA h g^{-1} retained at 200 mA g^{-1}. The capacity fading was 2% after 100 cycles for the PMMA-based electrolyte, compared to 20% for the liquid electrolyte.

Poly(triphenyl amine) (PTPA, **P16**) is another easily accessible polymer. Its theoretical Q_m (111 mA h g^{-1}) is much lower compared to PANI. Lu *et al.*[80] reported that the practical Q_m of PTPA in potassium half-cells approached ~100 mA h g^{-1} in the 2.0–4.0 V *vs.* K^+/K range, retaining 71 mA h g^{-1} after 60 cycles. In full cells with a graphite-based anode, the capacity reached 60 mA h g^{-1} at 50 mA g^{-1} per PTPA mass with a decent retention of 75.5% after 500 cycles. The average discharge potential was 3.2 V.

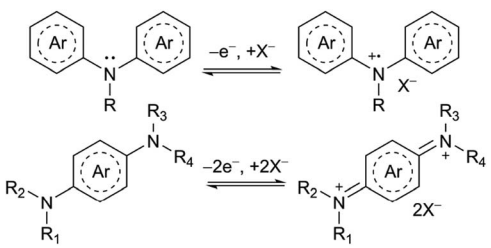

Scheme 3 Charge–discharge mechanisms for aromatic amine structural units.

In order to increase the capacity, Obrezkov *et al.*[81] proposed poly(*N*,*N*′-diphenyl-*p*-phenylenediamine) (PDPPD, **P17**), which is similar to PTPA but has higher theoretical Q_m (209 mA h g^{-1}). The experimental capacity, however, was only up to 63 mA h g^{-1} in the potential range of 2.5–4.2 *vs.* potassium. At the same time, the capacity of PDPPD was around 100 mA h g^{-1} in lithium and sodium cells, which indicates that the performance of K-based systems might be further improved.

Later, Obrezkov *et al.*[82] proposed a more successful poly(*N*-phenyl-5,10-dihydrophenazine) (PDPPZ, **P18**), which had the same theoretical Q_m but delivered several times higher practical capacity as compared to **P17**. After optimizing the electrolyte composition, *i.e.* using 2.2 M KPF_6 solution in diglyme, a Q_m of 162 mA h g^{-1} was reached at 200 mA g^{-1}. The average discharge potential was 3.6 V *vs.* K. Excellent rate capability (121 mA h g^{-1} at 10 A g^{-1}) was demonstrated along with decent cycling stability (59% retention after 2000 cycles at 2 A g^{-1}). Lately, Kapaev *et al.*[78] used DPPZ with a NaK-based anode and ~1.5 M KPF_6 solution in DME as the electrolyte, and demonstrated operation at even higher rates (65 mA h g^{-1} at 50 A g^{-1}).

Unlike other structures discussed in this section, poly(*N*-vinylcarbazole) (PVK, **P19**) is a pendant-type polymer with an aliphatic backbone. Li *et al.*[83] reported that Q_m for **P19** was up to 117 mA h g^{-1} at 20 mA g^{-1} in a 2.0–4.7 V *vs.* K range (average 4.0 V), close to the theoretical value of 138 mA h g^{-1}. At 2 A g^{-1}, the capacity reached 68 mA h g^{-1}, and 55% percent of it retained after 500 cycles.

2.6 Other structures

Gao and co-authors[71] have recently proposed CuDEPP **12**, a derivative of the copper(II) porphyrin complex, as a cathode material for potassium batteries. In the voltage range of 1.7–4.5 V *vs.* K, the first charge and discharge capacities were 2474 and 424 mA h g^{-1}, respectively. The coulombic efficiency (CE) was low (17%) due to the charging plateau appearing above 4.2 V, which was likely caused by the electrolyte decomposition. In subsequent cycles, the CE improved but the discharge capacity dropped to ~150–180 mA h g^{-1}.

The authors assumed that CuDEPP was undergoing two-electron reduction (CuDEPP-18π to CuDEPP-20π^{2-}) at lower potentials and two-electron oxidation (CuDEPP-18π to CuDEPP-16π^{2+}) at higher potentials. However, the charge–discharge profiles showed no pronounced features, appearing almost straight, supercapacitor-like[10] lines. At the same time, cyclic voltammograms of similar compounds are known to have a set of distinct peaks and a large voltage gap between p- and n-doping processes.[123–125] Considering a relatively large particle size of CuDEPP particles (>1 μm), it is unclear why it had such an electrochemical behavior.

The authors also demonstrated full cells with CuDEPP and graphene or bismuth as anodes. Particularly, the graphene-based full cells delivered a stable Q_m of ~50 mA h g^{-1} in

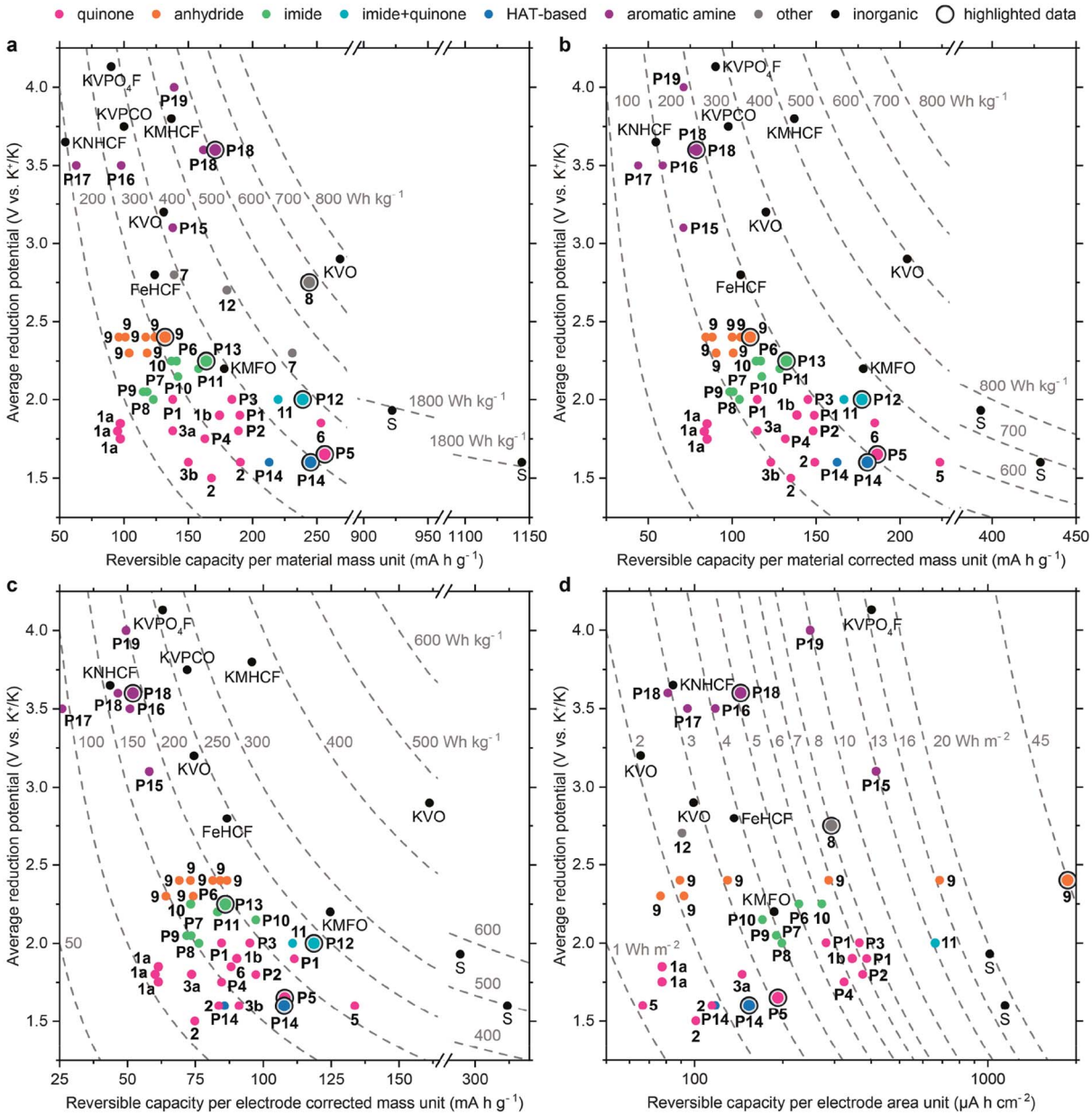

Chart 1 Average reduction (discharge) potentials *vs.* (a) material specific capacity Q_m, (b) material corrected specific capacity Q_m^{corr}, (c) electrode corrected specific capacity Q_e^{corr} and (d) electrode areal capacity Q_a for organic-based and selected inorganic cathode materials. Data points for the best organic-based materials of each type are highlighted. Material notations for highlighted data: **8** = CuTCNQ; **9** = PTCDA; **P5** = poly(-pentacenetetraone sulfide); **P13** = NTCDA-based poly(anthraquinonyl imide); **P14** = poly(hexaazatrinaphthylene); **P18** = poly(*N*-phenyl-5,10-dihydrophenazine) (PDPPZ). Notations for inorganic materials: FeHCF = $Fe[Fe(CN)_6]$; KMFO = $K_{0.7}Mn_{0.5}Fe_{0.5}O_2$; KMHCF = $K_{1.75}Mn[Fe(CN)_6]\cdot 0.16H_2O$; KNHCF = $K_{1.81}Ni[Fe(CN)_6]_{0.97}\cdot 0.086H_2O$; KVO = $K_{0.51}V_2O_5$ or $K_{0.42}V_2O_5\cdot 0.25H_2O$; KVPCO = $K_2[(VOHPO_4)_2(C_2O_4)]$.

a 0.01–3.8 V range. Unlike in most of the other cases discussed in this review, it was not reported that the anodes were pre-potassiated. Since there was no potassium source for the cathode metalation, the cells should have been operating in the dual-ion mode. The charge–discharge profiles were similar for the full cells and the half-cells.

2.7 Summary and perspective for cathode materials

The data for organic-based cathode materials are summarized in Table 1. All these compounds were reported for non-aqueous batteries, which should be mainly due to the mismatch between their working potentials and water stability voltage window. Some n-type materials, such as quinones[102] or aromatic imides,[86,103] can operate without decomposition of water, especially with highly concentrated electrolytes. However, their working potentials are close to the onset of the hydrogen evolution reaction,[126] which makes them more suitable for anodes rather than for cathodes (see Section 3.3). There are several reports on aromatic amines and nitroxyl radicals as cathodes for aqueous Li-,[127] Na-,[128] Zn-[129,130] and ammonium-based[131] cells. It might be expected

that similar K-based aqueous dual-ion batteries will become successful in the future.

As benchmark inorganic cathodes, we selected a number of materials for non-aqueous cells which, according to the reviews[17,24–35] and to the best of our knowledge, are superior in terms of voltage, specific energy/power or cycling stability and are attributed to various material families (hexacyanoferrates, layered oxides, polyanionic compounds, and conversion-type cathodes). The list of benchmarks includes $KVPO_4F$,[132] $K_2[(VOHPO_4)_2(C_2O_4)]$ (KVPCO),[133] $K_{1.75}Mn[Fe(CN)_6]\cdot 0.16H_2O$ (KMHCF),[134] $Fe[Fe(CN)_6]$ (FeHCF),[135] $K_{1.81}Ni[Fe(CN)_6]_{0.97}\cdot 0.086H_2O$ (KNHCF),[136] $K_{0.7}Mn_{0.5}Fe_{0.5}O_2$ (KMFO),[137] $K_{0.51}V_2O_5$ and $K_{0.42}V_2O_5\cdot 0.25H_2O$ (KVO),[138,139] and sulfur (S).[140,141]

Capacity and energy. The reversible capacities *vs.* average discharge (metalation) potentials for the materials are plotted in Chart 1a. Among organic materials, aromatic amines have the most attractive combination of high Q_m and high average discharge potentials, which technically provide higher specific energies (E_m) than most of the inorganic benchmarks.

It should be noted, however, that direct comparison of organic materials with the inorganic ones, which are metalated in the initial state, can be biased if only the capacity per material mass is considered. Organic materials are initially non-metalated and require additional potassium for proper operation, which decreases the real specific capacity. In dual-ion batteries, the supporting salt is decomposed during charging, so a significant part of it must be used in the cell, again limiting the real capacity. To avoid the bias, we calculated the capacity per material corrected mass (Q_m^{corr}), as discussed below.

If a rocking-chair type battery material was non-metalated in the initial state, Q_m^{corr} was calculated as follows:

$$Q_m^{corr} = Q_m\left(1 + \frac{Q_m}{F}M_{ci}\right)^{-1} \quad (1)$$

where F is Faraday constant (26 801.5 mA h mol^{-1}) and M_{ci} is the molar mass of the counter-ion with charge $z = 1$ (39.10 g mol^{-1} for K^+). For dual-ion cells, the molar mass of the potassium salt (KPF_6, 184.06 g mol^{-1}) was used instead of M_{ci}. Although the salt originated solely from the electrolyte in all reports dedicated to the organic materials, it is principally possible to use mixtures of solid salts and relatively small amounts of electrolyte.[142] For this reason, the total mass of the electrolyte was not considered.

For Q-TTF-Q **7**, CuTCNQ **8** and CuDEPP **12**, both rocking-chair and dual-ion mechanisms are considered possible (see Sections 2.2 and 2.6). The practical capacity proportion for these mechanisms is ambiguous, which makes the calculation of Q_m^{corr} challenging. Based on the proposed charge–discharge mechanisms,[62,63,71] the estimated Q_m^{corr} for **7** (Q_m = 231 mA h g^{-1}), **8** (Q_m = 244 mA h g^{-1}) and **12** (Q_m = 181 mA h g^{-1}) are 125, 109 and 103 mA h g^{-1}, respectively.

In case of KVOs, which contain some potassium in the initial state, Q_m^{corr} was calculated as follows:

$$Q_m^{corr} = Q_m\left(1 + \frac{Q_m - Q_m^{ic}}{F}M_{ci}\right)^{-1} \quad (2)$$

where Q_m^{ic} is the specific capacity of the material observed at the initial charge (the ratio between Q_m and Q_m^{ic} is considered constant at all current rates).

Additionally, we calculated the capacities per electrode corrected mass unit (Q_e^{corr}), which considers the mass of conductive additives and binders along with the mass of counter-ions or salts. Areal capacities (Q_a) were calculated in cases where the electrode mass loading was reported; if the loadings were reported as intervals, mean values were used (*e.g.*, 1.1 for 1.0–1.2 mg cm^{-2}).

As shown in Chart 1b, energy per material corrected mass unit (E_m^{corr}) is basically within the range of 200–350 W h kg^{-1} for all organic cathode materials, which is lower than for most of the benchmarks. Among organic compounds, quinones and HAT-based polymer **P14** have the largest capacities (Q_m^{corr} ~ 100–225 mA h g^{-1}) but relatively low potentials (1.6–2.0 V *vs.* K). Aromatic anhydrides and imides have higher potentials (2.0–2.3 V for imides and 2.3–2.4 V for anhydrides), and the capacities are close or lower than for quinones (Q_m^{corr} ~ 80–140 mA h g^{-1}). Aromatic amines, which are cathodes for dual-ion batteries, have the highest potentials (3.5–3.6 V), but using the heavy salt dramatically shrinks the Q_m^{corr} to 50–100 mA h g^{-1}.

If conductive fillers and binders are considered (Chart 1c), the capacity of organic materials further decreases compared to the inorganic benchmarks. For the organic cathodes, it is a common practice to use significant amounts of carbon black (30–50%, in contrast to 10–30% for inorganic analogs), and the electrode composition is typically left unoptimized. For conjugated polymers with decent intrinsic electron conductivities, it is expected that the carbon content might be decreased without drastically decreasing Q_m.

Areal capacities for organic-based cathodes range from ~0.07 to ~2 mA h cm^{-2} (Chart 1d). As in the case with the electrode composition, no optimization of the mass loading is typically performed. For PTCDA **9**, where such optimization took place,[67] record high areal capacity was demonstrated.

Volumetric capacity and density are usually unreported for organic materials used in potassium batteries. Density for solid polar organic compounds containing only C, H, N and O ranges between roughly 1.1 and 1.7 g cm^{-3},[143] and it is smaller than for inorganic cathode materials (calc. 2.3 g cm^{-3} for KMHCF,[134] calc. 3.1 g cm^{-3} for $KVPO_4F$,[144] and 3.35 g cm^{-3} for V_2O_5 (ref. 145)). This limits the applicability of organic cathode materials where the low device volume is crucial, *e.g.*, in portable electronics. However, in some electric vehicles and large-scale stationary applications the volume is supposed to be less restricted.

We suppose that both the capacities and the potentials of the reported organic cathodes can be significantly improved. Strategies for enhancing the specific energy, such as decreasing the content of electrochemically inactive units, introducing chelating or/and electron-deficient functional groups, *etc.*,[146] have not been widely applied for potassium cells.

Based on the recent advances in organic lithium batteries,[120,147] it might be suggested that a Q_m of 400 mA h g^{-1} is achievable for rocking-chair battery cathodes, which corresponds to an E_m^{corr} of about 400, 500 or 600 W h kg^{-1} if the average potential is 1.6, 2.0 or 2.4 V, respectively (Chart 2a).

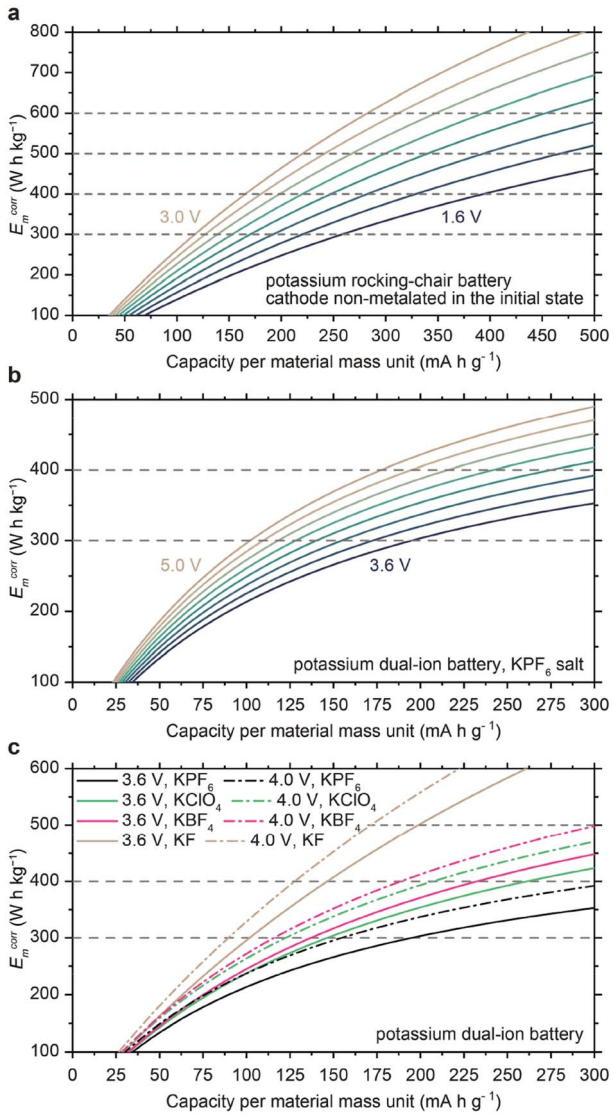

Chart 2 Energy per material corrected mass unit (E_m^{corr}) *vs.* capacity per cathode material mass unit (Q_m) for (a) potassium rocking-chair batteries with the average discharge voltage ranging from 1.6 to 3.0 V with a 0.2 V increment; (b) potassium dual-ion battery with KPF_6 as the supporting salt and the average discharge voltage ranging from 3.6 to 5.0 V with a 0.2 V increment; (c) dual-ion battery with different supporting salts and the average discharge voltages of 3.6 V (solid lines) or 4.0 V (dash-dotted lines).

For dual-ion batteries, increasing Q_m is also principally possible by, for example, increasing the concentration of redox-active nitrogen atoms in aromatic amines. For such optimized materials, where most of the active units are involved, it is expected that the operation potentials will get higher at least for conjugated structures because polymers with a high positive charge at the backbone are harder to oxidize. It will therefore be important to develop electrolytes for potassium batteries, which are tolerant to high voltages, or to elaborate protective coatings at the cathode surface. Certain progress in the development of high-voltage potassium battery electrolytes has already been achieved.[79,148–150]

However, in the extreme case, when Q_m of a dual-ion battery cathode is 300 mA h g^{-1} and the average potential is 5.0 V, E_m^{corr} is only ~500 W h kg^{-1} if KPF_6 is used as the supporting salt (Chart 2b). Switching to lighter salts, such as $KClO_4$, KBF_4 and particularly KF might significantly boost the energy density (Chart 2c). For potassium fluoride, an E_m^{corr} of ~500 W h kg^{-1} is achieved already at a reasonable ~200 mA h g^{-1} and 3.6 V. Optimization of the salt composition, however, has not been reported yet. Considering low solubility of KF in aprotic electrolytes, it is especially intriguing if it may succeed as the supporting salt.

Rate performance. Ragone plots for the best-performing organic and inorganic potassium battery materials are shown in Chart 3. In terms of specific energy and power calculated based on Q_m, Q_m^{corr} and Q_e^{corr}, polymers **P5**, **P14**, **P18** and the heat-treated PTCDA are highly competitive with the inorganic benchmarks. **P18** shows the best performance at the power of >3 kW kg^{-1} calculated per material corrected mass (Chart 3b). The key factors limiting the energy-power characteristics of the organic materials are low voltages (for rocking-chair type materials) and low Q_m^{corr} (for dual-ion batteries). Both parameters can be enhanced as discussed above.

Cycling stability. The data on cycling stability are plotted in Chart 4. The best stability for all non-aqueous batteries was reported for **P14**, which showed a decay of only 11% after 10 000 cycles at 10 A g^{-1}.[77] Cross-linked polymers show superior stability compared to small molecules and linear macromolecules because their solubility is negligible, provided that the molecular mass is sufficiently high.

Better cycling stability was generally observed for ether-based electrolytes (KPF_6 and KFSI solutions in DME). A number of studies shows that ether-based electrolytes are advantageous over carbonate-based ones.[55,67,72,77,82] To decrease the solubility of active materials, concentrated solutions, such as 3 M KFSI in DME, might be selected.

Selection of the anode material. Organic materials for rocking-chair batteries are typically non-metalated in the initial state, which narrows the list of appropriate anodes. The highest capacity is provided by metallic potassium (685 mA h g^{-1}). In concentrated KFSI-based solutions, plating-stripping of the pristine metal was reported to be highly reversible and dendrite-free due to the stable SEI, making the cells relatively safe.[150,151] Other strategies for eliminating dendrites, such as encapsulating the metal[152] or introducing an artificial SEI,[153] are also available. Liquid NaK-based anodes enable dendrite-free operation as well.[114] Graphite can serve as the anode if it is pre-potassiated, which can be done electrochemically or chemically, *e.g.*, by fusion with molten potassium.[154] For dual-ion batteries, there is no problem with using non-metalated anodes, since K^+ ions are provided by the supporting salt. Non-metalated organic-based anode materials are discussed in the following section.

3. Anode materials

3.1 Aryl carboxylates

Salts of aromatic dicarboxylic acids represent the most popular type of organic anode materials. They undergo reversible two-electron reduction forming enolates (Scheme 4). None of the studied aryl carboxylates are polymers (Fig. 2). For these

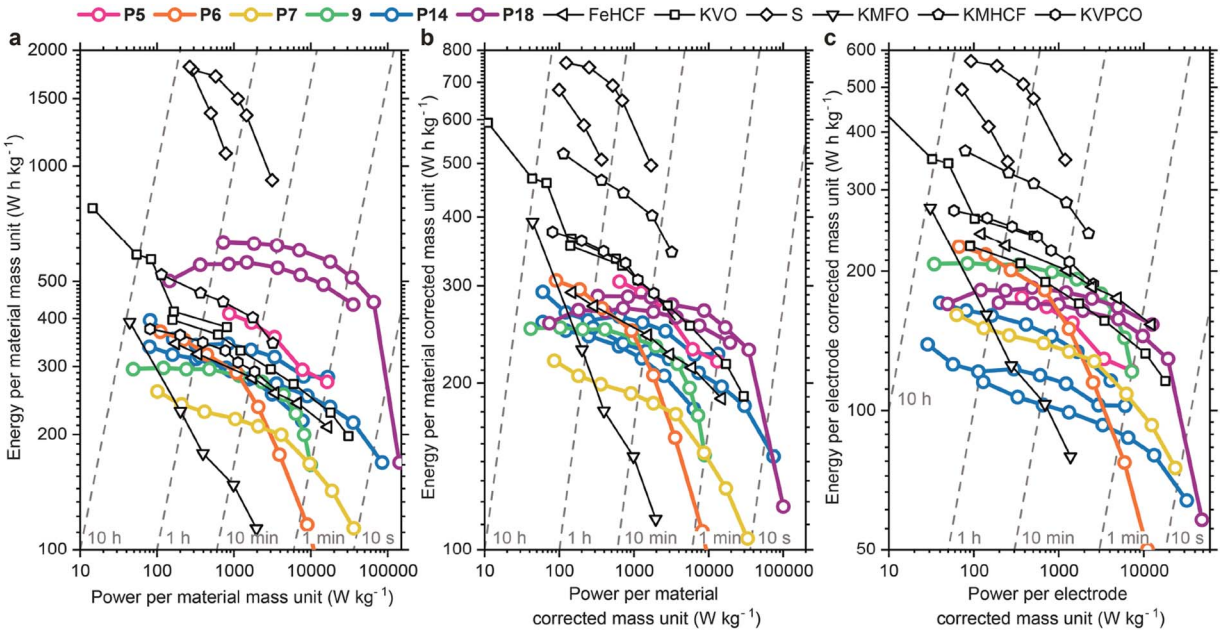

Chart 3 Ragone plots for high-power organic and inorganic cathode materials calculated based on (a) Q_m, (b) Q_m^{corr} and (c) Q_e^{corr}. Notations for organic materials: **9** = PTCDA; **P5** = poly(pentacenetetraone sulfide); **P6**, **P7** = polyimides derived from PTCDA and hydrazine (**P6**) or ethylene diamine (**P7**); **P14** = poly(hexaazatrinaphthylene); **P18** = poly(*N*-phenyl-5,10-dihydrophenazine) (PDPPZ).

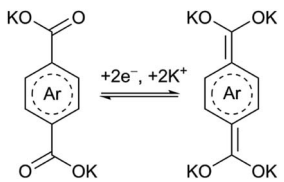

Scheme 4 Charge–discharge mechanism for aryl carboxylates.

compounds, the dissolution in non-aqueous electrolytes is limited owing to the ionic functionalities.

Salts of terephthalic acid are one of the simplest and cheapest compounds among dicarboxylic acid derivatives. Potassium terephthalate (K_2TP, **13a**) has a theoretical capacity of 221 mA h g^{-1}, which is relatively close to graphite (279 mA h g^{-1}). Its usage in potassium cells was first reported almost simultaneously by Li *et al.*[90] and Chen *et al.*[87] In both studies, the capacities were 260–270 mA h g^{-1}, which after subtracting the contribution from carbon additives resulted in ~210 mA h g^{-1} solely from **13a**. While Li *et al.*[90] used a solution of KFSI in EC : DMC as the electrolyte, Chen *et al.*[87] chose KPF_6 as the salt and showed that DME is a better solvent for reaching good stability and rate capability than carbonates. With 1 M KPF_6 in DME, the capacity at 1 A g^{-1} reached 185 mA h g^{-1}, and 94.6% of it was retained after 500 cycles. This decent performance was associated with a robust SEI, which was formed in the ether-based electrolyte but was lacking in the carbonate-based solutions.

Later, Chen *et al.*[89] used K_2TP under similar conditions as the anode for hybrid supercapacitors. Activated carbon was used as the cathode. Energy of 101 W h kg^{-1} and power of 2.16 kW kg^{-1} based on the mass of two electrodes were demonstrated. If the electrolyte mass was included, the values reached 41.5 W h kg^{-1} and 885 W kg^{-1}, respectively. The capacity retention of the supercapacitor was 97.7% in 500 cycles. In half cells, the capacity of K_2TP at 5 A g^{-1} was 124 mA h g^{-1}.

To further enhance the rate capability, composites of **13a** with CNTs[88] or GO[91] were proposed. The CNT-based composite showed particularly impressive results, with 130 mA h g^{-1} retaining at 12.5 A g^{-1}. In a full cell with this composite, the capacity of a potassium–iron hexacyanoferrate cathode was up to ~110 mA h g^{-1} with 90% retention after 60 cycles; at a high current rate of 2.6 A g^{-1}, 58 mA h g^{-1} was delivered.

As shown by Fan *et al.*,[92] free terephthalic acid **13b** can be used in anodes as well. However, acidic protons get substituted for potassium during the first cycle, causing large irreversible capacities and hydrogen release. Interestingly, the authors reported that only half of the H^+ are substituted for K^+, which is unexpected since both pK_{a1} and pK_{a2} of H_2TP are known to be high (3.5 and 4.8, respectively[155]). A similar situation was reported for **2**, as discussed in Section 2.1. This phenomenon should be further investigated and confirmed. Other properties of **13b**, such as capacities and charge–discharge profiles, were similar to **13a**.

Two reports were dedicated to cobalt-based terephthalates. Hu *et al.*[93] presented a layered MOF $Co_2(OH)_2TP$ **13c**. It showed a reversible capacity of up to 450 mA h g^{-1}, which stabilized at ~200–250 mA h g^{-1} after 10–20 cycles. At 1 A g^{-1}, ~131 mA h g^{-1} retained. According to XANES spectroscopy, Co^{2+} reversibly reduced to Co^0 along with the ligands, suggesting a theoretical capacity of 339 mA h g^{-1}. However, the observed higher experimental capacity was not explained and

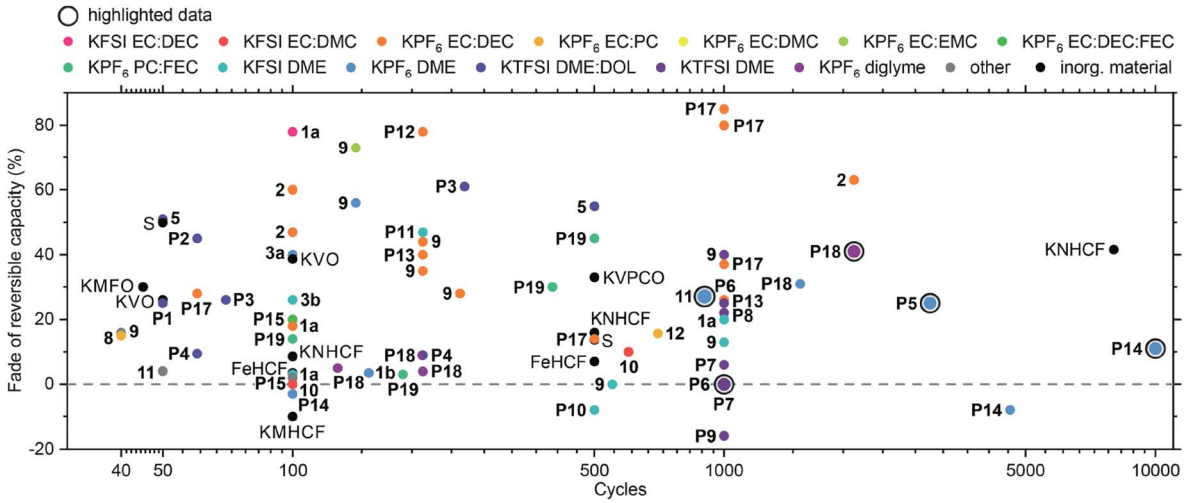

Chart 4 Cycling stability for organic-based and inorganic cathode materials. For organic-based materials, utilized electrolytes are color-coded. Data points for the best organic materials of each type are highlighted. Material notations for highlighted data: **11** = PTCDI derivative with anthraquinone moieties (PTCDI-DAQ); **P5** = poly(pentacenetetraone sulfide); **P6**, **P7** = polyimides derived from PTCDA and hydrazine (**P6**) or ethylene diamine (**P7**); **P14** = poly(hexaazatrinaphthylene); **P18** = poly(*N*-phenyl-5,10-dihydrophenazine) (PDPPZ).

might be partially attributed to acetylene black, whose contribution to the capacity was not considered.

Li *et al.*[94] studied the electrochemical behavior of cobalt terephthalate (CoTP, **13d**). Pristine CoTP showed a small reversible capacity of ~110 mA h g^{-1}. To improve the performance, it was ball-milled with additional carbon, which decreased the particle size and enhanced electronic conductivity. This composite delivered up to ~240 mA h g^{-1} of the reversible capacity and showed a moderate rate and cycle performance. The authors proposed that CoTP irreversibly transformed into Co^0 and K_4TP, with only the latter being electrochemically active in the subsequent cycles.

As mentioned in Section 1, cobalt is a rare and expensive element, so its use in practical applications should be avoided where possible. Deng *et al.*[95] proposed using an iron terephthalate-derived MOF-235, or $[Fe_3O(TP)_3(DMF)_3][FeCl_4](DMF)_3$ **13e**, which is apparently more sustainable than **13c** and **13d**. In a composite with CNTs, a capacity of up to 234 mA h g^{-1} was reported along with moderate rate and cycling capabilities. Based on the XPS data, the authors proposed that only the terephthalate ligands got reduced upon potassiation, while Fe^{3+} were left intact even at ~0 V *vs.* K^+/K. We doubt the proposed mechanism and suggest that it should be further studied with bulk analytical techniques, such as Mössbauer spectroscopy.

Several other potassium carboxylates were studied as potassium battery anodes. Li *et al.*[90] reported that potassium pyridinedicarboxylate **14** behaved similar to terephthalate, with the charge–discharge plateaus observed at slightly higher voltages due to the electron-withdrawing heteroatom.

Later, Li *et al.*[96] proposed biphenyl- and stilbene-derived dicarboxylates **15** and **16**. Their charge–discharge profiles were also similar to K_2TP. The materials delivered 130–150 mA h g^{-1} at 10 mA g^{-1} and had modest rate performance. To improve it, the authors added 5% wt. of graphene. As a result, the capacities at 1 A g^{-1} increased to 99 and 66 mA h g^{-1} for **15** and **16**, respectively. After 3000 cycles, ~40% of the initial capacity was retained for **15**. At low currents, the capacities (>200 mA h g^{-1}) were higher than theoretically predicted, likely due to the contribution from the carbon additives.

Recently, Li *et al.*[97] also explored naphthalene dicarboxylate **17**, which behaved similar to the previous compounds. It had a reversible capacity of up to ~200 mA h g^{-1} at 10 mA g^{-1}, which decreased to 55 mA h g^{-1} at 500 mA g^{-1}. By adding CNTs, the capacity at 0.5 A g^{-1} increased to 76 mA h g^{-1}.

Perylene tetracarboxylate **18**, which was studied by Fan *et al.*,[98] had a depotassiation plateau at 1.3–1.5 V *vs.* K^+/K, which was considerably higher than for dicarboxylates (0.6–0.8 V). After subtracting the contribution from carbon additives, the experimental capacity was 76 mA h g^{-1} at 100 mA g^{-1}. It was shown that only two carboxyls per molecule were electrochemically active, limiting the theoretical capacity to 93 mA h g^{-1}. Apparently, after two carbonyls are reduced, their negative charge strongly decreases the reduction potential of the other two groups. On the other hand, non-metalated carboxyls are electron-withdrawing and therefore increase the redox potentials, making the anode energetically less favorable.

Overall, potassium terephthalate is by far the most attractive representative of the aryl carboxylate family. It has the highest capacity, which can be maintained at fast charge–discharge *via* making composites with CNTs and possibly other conductive additives. Additionally, it is cheap and has very low toxicity (LD_{50} > 5 g kg^{-1} for H_2TP).[156]

3.2 Azo compounds

Azo compounds, particularly aromatic ones, might undergo two-electron reversible N=N group reduction,[157–160] as depicted in Scheme 5.

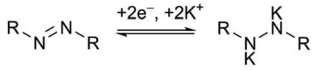

Scheme 5 Charge–discharge mechanism for azo compounds.

Wang *et al.*[99] studied azobenzene-4,4′-dicarboxylic acid potassium salt (APADTS, **19**) at various temperatures. In the 0.5–3.0 V range, charge–discharge profiles of APADTS had one plateau from 1.3–1.5 V *vs.* K^+/K, and the carboxyls were considered electrochemically inactive. At r.t., the reversible capacity reached 134 mA h g^{-1} at 15.5 mA g^{-1}, and 86/66 mA h g^{-1} was retained at 155/1550 mA g^{-1}, respectively. At elevated temperatures (50 or 60 °C) the capacities increased. For example, 138 mA h g^{-1} was observed at 155 mA g^{-1} and 50 °C. Decent cycling stability was demonstrated at r.t. and 50–60 °C.

Xu *et al.*[100] tested azobisisobutyronitrile (AIBN, **20**) in a wider voltage range of 0.01–3.0 V *vs.* K^+/K. The first reversible capacity was 260 mA h g^{-1} at 5 mA g^{-1}, but it quickly faded during five cycles; 65 mA h g^{-1} was observed at 50 mA g^{-1}. Charge–discharge profiles had no obvious plateaus, and most of the capacity was released below 1.5 V *vs.* K^+/K.

3.3 Aromatic anhydrides, imides and quinones

Although quinones, aromatic anhydrides and imides are typically used for cathodes (see Section 2), several reports on using them as anode materials were published. Hu *et al.*[64] reported that PTCDA **9** might accept up to 11 potassium ions when reduced to 0.01 V *vs.* K^+/K, resulting in a large initial capacity of ~900 mA h g^{-1} at 10 mA g^{-1}. However, a significant part of it was irreversible, with ~410 mA h g^{-1} delivered during the following depotassiation up to 3.0 V. It is unclear what percentage of the irreversible capacity should be attributed to the reduction of PTCDA and not to the SEI formation. After 35 cycles, the capacity dropped to ~140 mA h g^{-1}.

Later, Pan *et al.*[85] demonstrated much better performance for PTCDI **10**. With 1 M KPF_6 in DME, a stable reversible capacity of ~300 mA h g^{-1} was demonstrated at 0.5 A g^{-1} in the 0.01–3.0 V range. Even at 5 A g^{-1}, 208 mA h g^{-1} was delivered. However, the performance was poor in a carbonate-based electrolyte, which stresses the importance of the suitable electrolyte selection. It was proposed that six K^+ per PTCDI molecule were reversibly stored. All carbonyls were supposedly reduced, and two extra metal ions resided at the aromatic rings. This proposed mechanism, however, needs to be further investigated. As a feasible alternative, small clusters of metallic potassium can be formed in the matrix of the active material at low discharge potentials of ~0 *vs.* K^+/K.

PTCDI can also be successfully used in aqueous batteries, as reported by Hu *et al.*[86] The authors selected a superconcentrated 22 M KCF_3SO_3 electrolyte to suppress hydrogen evolution at a potential of −1.3 V *vs.* Ag/AgCl. PTCDI delivered 125 mA h g^{-1} at 65 mA g^{-1} and 110 mA h g^{-1} at 2.6 A g^{-1}. It had a decent capacity retention of 77% after 1000 cycles. A full cell with a $K_xFe_yMn_{1-y}[Fe(CN)_6]_w \cdot zH_2O$-based cathode and the PTCDI-based anode showed the energy density of 80 W h kg^{-1} based on the mass of both electrodes, which was higher than for previously reported aqueous Na- and K-ion batteries. Moreover, it had a remarkable capacity retention of 73% after 2000 cycles at 0.52 A g^{-1}, as well as high capacities in a wide temperature range (−20 to 60 °C).

Later, Wang *et al.*[84] published a similar study, using annealed PTCDA as the anode material and 30 M KFSI aqueous solution as the electrolyte. The reversible capacity of PTCDA reached 134 mA h g^{-1} at 0.2 A g^{-1}. Decent rate and cycling capabilities were demonstrated. A full cell with potassium iron(II) hexacyanoferrate as the cathode delivered 39 mA h g^{-1} based on the combined mass of the electrodes, and it was almost constant up to 4 A g^{-1} current density. The capacity retention of the full cell was 89% after 1000 cycles at 2 A g^{-1}.

Li and co-authors[103] applied PTCDA-derived polymer **P10** as the anode for aqueous K-ion batteries. Saturated solutions of K_2SO_4 (~0.69 M) or KNO_3 (~3.75 M) were tested as the electrolytes. The potassium nitrate solution enabled better rate capabilities with **P10** as the active material, owing to the higher conductivity. Particularly, ~90 mA h g^{-1} was delivered at 5.4 A g^{-1}, which was about 70% of the value achieved at 0.36 A g^{-1}. A full cell with the potassium hexacyanoferrate cathode had an energy density of 24.2 W h kg^{-1} (per mass of both electrodes), could reach a high power of 2.08 kW kg^{-1}, and retained 74% of the capacity after 300 cycles.

Regarding the quinone-based materials, Chen *et al.*[101] tested menadione (vitamin K3, **21**) in a 0.1–2.5 V *vs.* K^+/K range. In a composite with CNTs, it showed a capacity of 256 mA h g^{-1} at 50 mA g^{-1} and delivered 165 mA h g^{-1} at 1 A g^{-1}. No plateaus were observed in the charge–discharge profiles. This is atypical for small-molecule quinones, which basically have a distinct signature of two-electron reversible reduction.[102,161,162] The reasons for such behavior are unclear. Relatively high stability over one hundred cycles was demonstrated, which is also unusual for highly soluble molecules and is possibly caused by their strong adsorption on the carbon additive surface.

Yao *et al.*[102] presented a series of aqueous systems with quinone-based anodes and industrially established cathodes, which showed excellent stability, kinetics and energy density. Particularly for K-based batteries, PAQS **P1** was paired with $Ni(OH)_2$ in alkaline media (10 M KOH). The anode showed a capacity of 200 mA h g^{-1}. At r.t., the full cell energy density (79 W h kg^{-1}/138 W h L^{-1}) was smaller than for a nickel metal hydride battery (180 W h kg^{-1}/597 W h L^{-1}), partially due to a relatively high anode potential. However, the capacity retention (88% after 1300 cycles) was better than for the best metal hydrides. Moreover, the capacity of PAQS decreased only by 7% as the temperature decreased from 25 to −25 °C. It is in contrast with Ni-MmH, whose energy density significantly decreases at lower temperatures.

3.4 Other structures

Jiang *et al.*[104] proposed a series of conjugated microporous polymers **P20–P25**, which contained aromatic and optional benzothiadiazole units. Among them, **P23** delivered the highest reversible capacity of 428 mA h g^{-1} at 30 mA g^{-1} (358 mA h g^{-1} after subtracting the carbon contribution). Moderate rate performance (104 mA h g^{-1} at 0.5 A g^{-1}) and good cycling

stability (272 mA h g^{-1} after 500 cycles at 50 mA g^{-1}) were demonstrated. The proposed mechanism included potassiation of both benzothiadiazole and pyrene units.

Another microporous polymer **P26** was studied by Wang *et al.*[105] A composite of this boronic ester with CNTs delivered up to 330 or 68 mA h g^{-1} at 25 and 5000 mA g^{-1}, respectively. Decent cycling stability was also shown: 161 mA h g^{-1} was retained after 4000 cycles at 1 A g^{-1}. Without CNTs, the capacity was low.

Several triazine-based frameworks **P27–P29** have been recently explored in potassium cells. Zhu *et al.*[106] showed that the capacity of **P27** was very low (<100 mA h g^{-1}) because the pore size (0.5 nm) was too small to accommodate multiple potassium ions. **P28**, which had larger pores, had reversible capacities of up to 152 and 53 mA h g^{-1} at 50 and 1000 mA g^{-1}, respectively.

Lately, Wang *et al.*[107] proposed **P29**, a fluorinated analog of **P28**. To enhance its performance, the authors exfoliated the particles

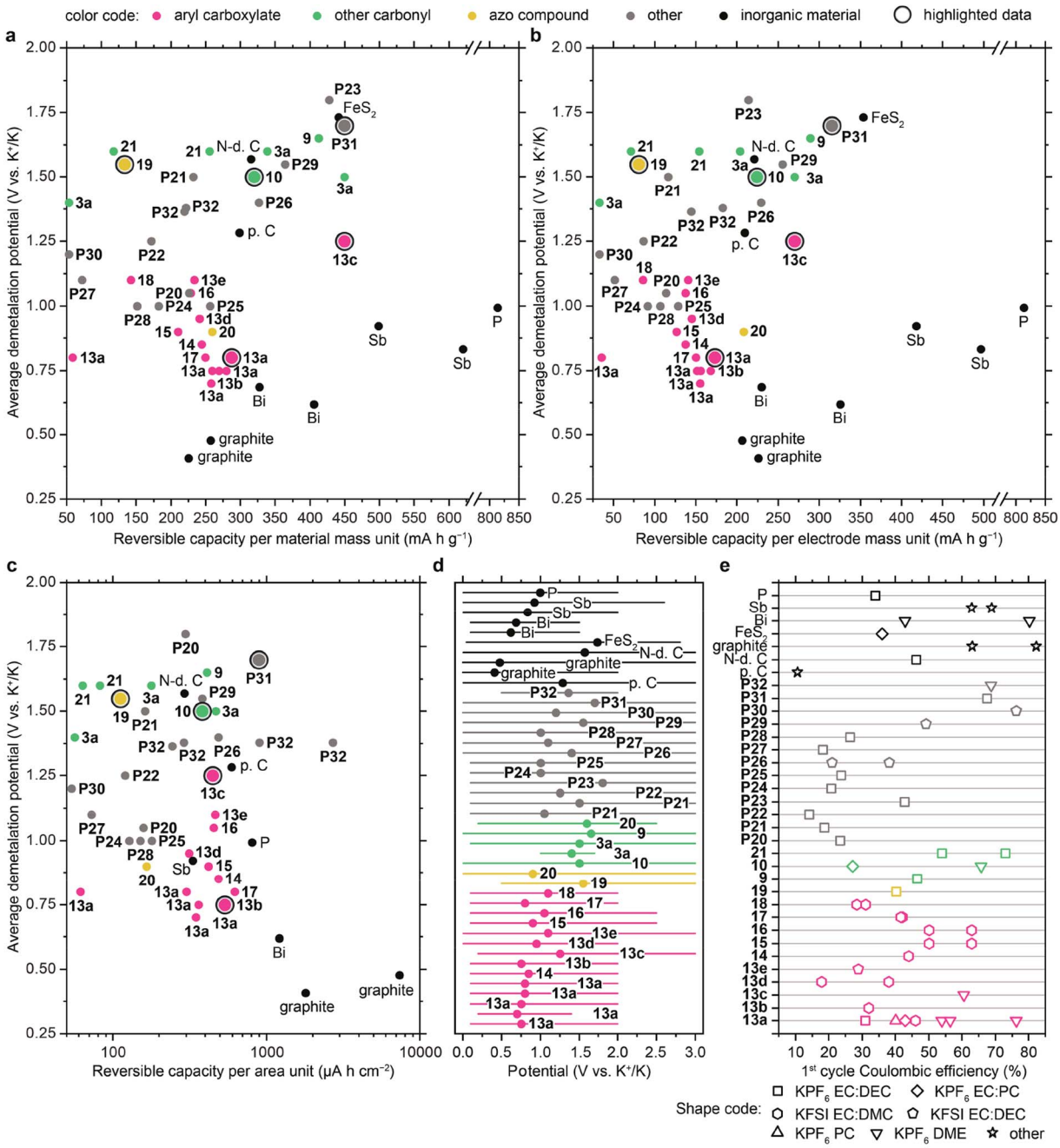

Chart 5 Average demetalation potentials *vs.* (a) material specific capacity Q_m, (b) electrode specific capacity Q_e and (c) electrode areal capacity Q_a for organic-based and selected inorganic anode materials; (d) reported potential windows and average demetalation potentials; (e) 1st cycle coulombic efficiencies in different electrolytes. Data points for the best organic materials of each type are highlighted. Material notations for highlighted data: **10** = PTCDI; **13a** = potassium terephthalate; **13c** = cobalt terephthalate-hydroxide; **19** = azobenzene-4,4′-dicarboxylic acid potassium salt (ADAPTS).

via ball-milling. The resulting material delivered a charge capacity of up to ~450 mA h g^{-1} at 100 mA g^{-1}, which after 20 cycles stabilized at ~250 mA h g^{-1}, reaching 228 mA h g^{-1} after 200 cycles. At 2 A g^{-1}, 58 mA h g^{-1} was delivered.

Feng *et al.*[108] reported that polythiophene (PTh, **P30**) had a low capacity of 58 mA h g^{-1} in a 0.0–3.0 V *vs.* K^+/K range. Considering that the contribution from carbon black was not subtracted, it is questionable whether polythiophene was electrochemically active at all. It is known that only low n-doping levels are typically achievable for PTh,[163] which is a possible explanation of its poor performance in the potassium battery anodes.

Zhang *et al.*[109] demonstrated high reversible capacities (up to 450 mA h g^{-1} at 50 mA g^{-1}) for poly(*o*-phenylene diamine) **P31** in a 0.01–3.0 V *vs.* K^+/K range. The performance was dependent on the ratio of phenylene diamine and $(NH_4)_2S_2O_8$, which were used for the synthesis. The best material was stable over 200 cycles and delivered 73 mA h g^{-1} at 2 A g^{-1}. As proposed by the authors, potassium bound with nitrogen atoms of the material during reduction.

Recently, Kapaev *et al.*[110] showed that **P32**, a nickel-based polymer derived from 1,2,4,5-benzenetetramine, had the capacity of 220 mA h g^{-1} in a 0.5–2.0 V *vs.* K^+/K range. High rate capabilities of up to 104 mA h g^{-1} at 10 A g^{-1} were demonstrated along with decent cycling stability (4% decay after 200 cycles). In addition, high areal capacity of 2.73 mA h cm^{-2} was reported. The charge–discharge mechanism apparently included two-electron reduction of the ligand, which was accompanied by two phase transitions, as evidenced by *in situ* XRD.

3.5 Summary and perspective for anode materials

The data for organic-based anode materials are provided in Table 2. Only a few reports,[84,86,102,103] which were discussed in Section 3.3, were dedicated to aqueous batteries. For this reason, the summary and outlook will be focusing on the non-aqueous systems. As in the case of cathode materials (Section 2.7), we chose several inorganic benchmarks, which showed superior capacities, rate capabilities or cycling stability. These benchmarks include graphite,[149,164] porous carbon (p. C),[165] N-doped carbon (N-d. C),[166] bismuth,[167,168] antimony,[169,170] iron disulfide[171] and red phosphorous.[172]

Capacity, potentials and coulombic efficiencies. Reversible capacities (Q_m) *vs.* average charge (demetalation) potentials are shown in Chart 5a. The capacities of organic-based materials typically lay within 200–350 mA h g^{-1}, with the average potentials ranging between 0.7 and 1.5 V. Aryl dicarboxylates have the lowest potentials, owing to the pronounced plateaus at 0.6–0.8 V *vs.* K^+/K. For most other materials, a significant portion of the charge capacity is released above 1 V, which decreases the energy density of the full cells.

It should be noted that contribution from carbon additives, which are also electrochemically active at low potentials and generally constitute 20–30% wt. of the electrodes, is typically not considered while calculating Q_m. For comparison with the inorganic benchmarks, it is better to consider the capacities per electrode mass (Q_e), as shown in Chart 5b.

Compared with graphite, Bi, Sb and P, organic-based materials are less attractive in terms of the potentials. The electrode capacities are also generally lower, although several materials with high demetalation potentials showed a Q_e of above 250 mA h g^{-1}. Areal capacities (Chart 5c) are mostly comparable for organic-based materials and the benchmarks, except for graphite, for which very high loadings (up to 28.56 mg cm^{-2}, corresponding to ~7.4 mA h cm^{-2}) were demonstrated. Similar to the cathodes (Section 2.7), the material loading of the anodes is typically left unoptimized.

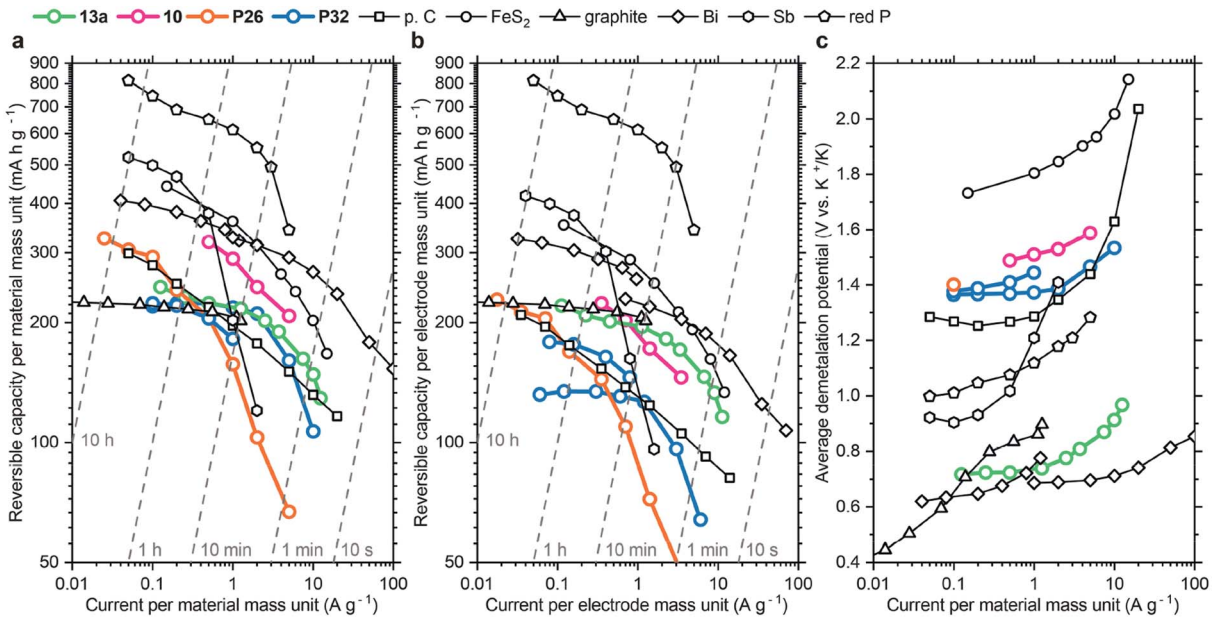

Chart 6 Q_m (a), Q_e (b) and average demetalation potentials (c) *vs.* specific current for selected organic-based and inorganic anode materials. Notations for organic-based materials: **10** = PTCDI; **13a** = potassium terephthalate; **P26** = boronic-ester based COF; **P32** = Ni-based coordination polymer derived from tetraaminobenzene.

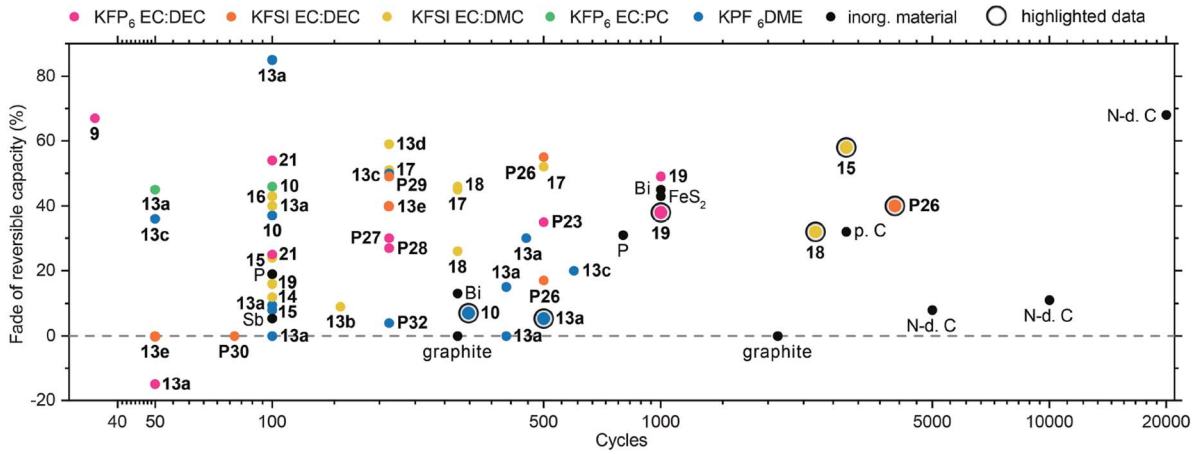

Chart 7 Cycling stability for organic-based and inorganic anode materials. For organic-based materials, utilized electrolytes are color-coded. Material notations for highlighted data: **10** = PTCDI; **13a** = potassium terephthalate; **15** = potassium biphenyl carboxylate; **18** = perylene tetracarboxylate; **19** = azobenzene-4,4′-dicarboxylic acid potassium salt (ADAPTS).

Working potential ranges, particularly the lowest potentials, might be important for safety considerations. At low potentials (~0 V *vs.* M^+/M), there is a risk of metal deposition at the anode, which might be caused by overcharge, fast charging or low temperatures. Alkali metals tend to form dendrites, which cause dangerous short-circuiting. The metal deposition phenomenon is known for lithium-ion batteries,[173,174] and expected to be possible in potassium-based cells. Moreover, materials at low potentials are also highly reactive, which raises safety concerns in case of possible leakages and increased temperatures.[175]

As shown in Chart 5d, most of the materials get metalated down to ~0 V *vs.* K^+/K. However, there are three compounds, **3a**, **19** and **P32**, which work in presumably safe potential ranges (1.0–1.7, 0.5–3.0 and 0.5–2.0 V, respectively). Among them, **P32** showed the highest capacity along with decent rate and cycle performance. Its electrochemical characteristics are similar to renowned lithium titanites.[175] Purely inorganic materials with decent properties, which work in safe potential ranges, are not reported yet.

While increasing the anode potentials can make the batteries safer, it also lowers their energy density. Lowering the average demetalation potential is another direction for developing organic-based anodes. It can be done, for example, by adding electron-donating substituents, such as methyl or methoxy units, to the aromatic rings of carboxylates and other molecules.

The critical property of anode materials is coulombic efficiency. CE at the first cycle is particularly significant since it usually leads to the highest capacity losses due to SEI formation and other irreversible reduction processes. As shown in Chart 5e, a relatively high 1st cycle CE (>60%) is observed for carboxylates, carbonyls **10** and **21**, as well as for **P30**, **P31**, and **P32**. For other materials, as well as for some inorganic benchmarks (carbons with a high surface area, phosphorous, FeS_2), the CE is even lower. It should be noted that the CE depends not only on the material but also on the electrolyte composition. The tuning of the electrolyte is rarely reported. Some studies indicate that using ether-based electrolytes, such as KPF_6 in DME, improves the CE.[85,87] More attention should be paid to the electrolyte optimization, particularly for the materials that showed low CE with the carbonate-based solutions.

Rate performance. Dependencies of Q_m, Q_e and average potentials on the specific current are shown for the best-performing materials in Chart 6. Among organic-based materials, potassium terephthalate with CNTs showed the best combination of high-rate capacities and low potentials. This result is comparable with some advanced inorganic materials. The performance of **10**, **P26** (as a composite with CNTs) and **P32** is close to porous carbon when charged in 10 min or slower.

For small molecules, making composites with conductive fillers is one of the main strategies to enhance the rate capability. Decreasing the particle size, *e.g.*, *via* ball-milling, is apparently another effective approach. Conjugated polymers should have better electron conductivity and potentially perform better than non-conductive small molecules. However, the performance of reported conjugated structures was generally moderate. We suppose that this is partly because non-optimal carbonate-based electrolytes were used with these materials.

Cycling stability. Data on the stability are shown in Chart 7. High stabilities were achieved for polymers and small-molecule carboxylates, which are insoluble due to their ionic functionalities. However, for graphite and N-doped carbon even slower capacity fading rates were reported. Several studies showed that ether-based electrolytes were better for stability than carbonate-based solutions, provided that KPF_6 was used as the salt.[85,87] At the same time, the largest number of cycles among organic anodes (**15**, **18**, **P26**) was achieved using the electrolyte composed of 1 M KFSI in EC : DEC or EC : DMC. Further investigation of the electrolyte effects is important for minimizing the capacity fading rate.

4. Conclusion

To summarize, multiple organic-based active materials showed promising characteristics in potassium-based batteries. Their

capacities and potentials are typically less attractive than those of the state-of-the-art inorganic analogs, but the demonstrated rate and cycle capabilities make them highly competitive. There are still plenty of opportunities to improve the characteristics of the organic-based compounds using the truly unlimited diversity of molecular structures and tunability of their properties *via* functional group substitution. New advanced cathode and anode materials can be developed *via* rational molecular design, morphology optimization, engineering conductive fillers, and tuning the electrolyte composition.

Abbreviations

AB	Acetylene black
AC	Activated carbon
ADAPTS	Azobenzene-4,4′-dicarboxylic acid potassium salt
1,5-AQDS	Anthraquinone-1,5-disulfonic acid disodium salt
2,6-AQDS	Anthraquinone-2,6-disulfonic acid disodium salt
CB	Carbon black
CE	Coulombic efficiency
CMC	Sodium carboxymethyl cellulose
CNT	Carbon nanotubes
COF	Covalent organic framework
CuDEPP	[5,15-Bis(ethynyl)-10,20-diphenylporphinato] copper
CuTCNQ	Copper-tetracyanoquinodimethane
DEC	Diethyl carbonate
DMC	Dimethyl carbonate
DME	1,2-Dimethoxyethane
DMF	*N*,*N*-Dimethylformamide
DOL	1,3-Dioxolane
EC	Ethylene carbonate
EMC	Ethyl methyl carbonate
FEC	Fluoroethylene carbonate
FeHCF	$Fe[Fe(CN)_6]$
FTIR	Fourier-transform infrared
GO	Graphene oxide
HAT	Hexaazatriphenylene
KB	Ketchen black
KFHCF	Potassium iron(II) hexacyanoferrate
KFSI	Potassium bis(fluorosulfonyl) imide
KMFO	$K_{0.7}Mn_{0.5}Fe_{0.5}O_2$
KMHCF	$K_{1.75}Mn[Fe(CN)_6]\cdot 0.16H_2O$
KNHCF	$K_{1.81}Ni[Fe(CN)_6]_{0.97}\cdot 0.086H_2O$
KTFSI	Potassium bis(trifluoromethanesulfonyl) imide
KVO	$K_{0.51}V_2O_5$ or $K_{0.42}V_2O_5\cdot 0.25H_2O$
KVPCO	$K_2[(VOHPO_4)_2(C_2O_4)]$
LD_{50}	Median lethal dose
LIB	Lithium-ion battery
LiTFSI	Lithium bis(trifluoromethanesulfonyl) imide
MOF	Metal–organic framework
N-d. C	N-Doped carbon
n.r.	Not reported
Ni-MmH	Nickel metal hydride battery
NTCDA	Naphthalenetetracarboxylic dianhydride
p. C	Porous carbon
PAI	Polyamide-imide
PANI	Polyaniline
PAQS	Poly(anthraquinonyl sulfide)
PC	Propylene carbonate
PDPPD	Poly(*N*,*N*′-diphenyl-*p*-phenylenediamine)
PDPPZ	Poly(*N*-phenyl-5,10-dihydrophenazine)
PMMA	Poly(methyl methacrylate)
PPD	*p*-Phenylene diamine
PPTS	Poly(pentacenetetraone sulfide)
PTCDA	Perylenetetracarboxylic dianhydride
PTCDI	3,4,9,10-Perylene-tetracarboxydiimide
PTCDI-DAQ	*N*,*N*′-Bis(2-anthraquinone)]-perylene-3,4,9,10-tetracarboxydiimide
PTFE	Poly(tetrafluoroethylene)
PTh	Polythiophene
PTPA	Poly(triphenyl amine)
PVdF	Poly(vinylidene fluoride)
PVK	Poly(*N*-vinylcarbazole)
$Pyr_{13}FSI$	*N*-Propyl-*N*-methylpyrrolidinium bis(fluorosulfonyl)imide
Q-TTF-Q	[2,2′-Bibenzo[*d*][1,3]dithiolylidene]-4,4′,7,7′-tetraone
r.t.	Room temperature
SA	Sodium alginate
SEI	Solid electrolyte interphase
SEM	Scanning electron microscopy
SP	Super P
TP	Terephthalate
XANES	X-ray absorption near edge structure
XRD	X-ray diffraction

Notes

During the peer review process for this paper, another manuscript on a similar topic[176] was accepted for publication in *Journal of Materials Chemistry A*.

Conflicts of interest

There are no conflicts to declare.

Acknowledgements

The reported study was funded by RFBR, project number 19-33-90034. General support was also provided by the Russian Ministry of Science and Education (project 0089-2019-0010/No. AAAA-A19-119071190044-3) at IPCP RAS.

References

1 M. Li, J. Lu, Z. Chen and K. Amine, *Adv. Mater.*, 2018, **30**, 1800561.
2 R. Schmuch, R. Wagner, G. Hörpel, T. Placke and M. Winter, *Nat. Energy*, 2018, **3**, 267–278.
3 X. Zeng, M. Li, D. Abd El-Hady, W. Alshitari, A. S. Al-Bogami, J. Lu and K. Amine, *Adv. Energy Mater.*, 2019, **9**, 1900161.
4 G. E. Blomgren, *J. Electrochem. Soc.*, 2017, **164**, A5019–A5025.

5 G. Martin, L. Rentsch, M. Höck and M. Bertau, *Energy Storage Materials*, 2017, **6**, 171–179.
6 A. Battistel, M. S. Palagonia, D. Brogioli, F. La Mantia and R. Trócoli, *Adv. Mater.*, 2020, 1905440, DOI: 10.1002/adma.201905440.
7 N. Yabuuchi, K. Kubota, M. Dahbi and S. Komaba, *Chem. Rev.*, 2014, **114**, 11636–11682.
8 M. D. Slater, D. Kim, E. Lee and C. S. Johnson, *Adv. Funct. Mater.*, 2013, **23**, 947–958.
9 C. Vaalma, D. Buchholz, M. Weil and S. Passerini, *Nat. Rev. Mater.*, 2018, **3**, 18013.
10 T. B. Schon, B. T. McAllister, P.-F. Li and D. S. Seferos, *Chem. Soc. Rev.*, 2016, **45**, 6345–6404.
11 N. Matsuura, K. Umemoto and Z. i. Takeuchi, *Bull. Chem. Soc. Jpn.*, 1974, **47**, 813–817.
12 S. Komaba, T. Hasegawa, M. Dahbi and K. Kubota, *Electrochem. Commun.*, 2015, **60**, 172–175.
13 P. Ge and M. Fouletier, *Solid State Ionics*, 1988, **28–30**, 1172–1175.
14 K. Nobuhara, H. Nakayama, M. Nose, S. Nakanishi and H. Iba, *J. Power Sources*, 2013, **243**, 585–587.
15 K. Kubota, M. Dahbi, T. Hosaka, S. Kumakura and S. Komaba, *Chem. Rec.*, 2018, **18**, 459–479.
16 T. A. Pham, K. E. Kweon, A. Samanta, V. Lordi and J. E. Pask, *J. Phys. Chem. C*, 2017, **121**, 21913–21920.
17 W. Zhang, Y. Liu and Z. Guo, *Sci. Adv.*, 2019, **5**, eaav7412.
18 H. Maleki and J. N. Howard, *J. Power Sources*, 2006, **160**, 1395–1402.
19 P. Arora, R. E. White and M. Doyle, *J. Electrochem. Soc.*, 1998, **145**, 3647–3667.
20 R. Guo, L. Lu, M. Ouyang and X. Feng, *Sci. Rep.*, 2016, **6**, 30248.
21 S. Muench, A. Wild, C. Friebe, B. Häupler, T. Janoschka and U. S. Schubert, *Chem. Rev.*, 2016, **116**, 9438–9484.
22 T. Janoschka, M. D. Hager and U. S. Schubert, *Adv. Mater.*, 2012, **24**, 6397–6409.
23 P. Poizot, J. Gaubicher, S. Renault, L. Dubois, Y. Liang and Y. Yao, *Chem. Rev.*, 2020, **120**, 6490–6557.
24 Y.-S. Xu, S.-Y. Duan, Y.-G. Sun, D.-S. Bin, X.-S. Tao, D. Zhang, Y. Liu, A.-M. Cao and L.-J. Wan, *J. Mater. Chem. A*, 2019, **7**, 4334–4352.
25 Q. Zhang, Z. Wang, S. Zhang, T. Zhou, J. Mao and Z. Guo, *Electrochem. Energy Rev.*, 2018, **1**, 625–658.
26 T. Hosaka, T. Shimamura, K. Kubota and S. Komaba, *Chem. Rec.*, 2019, **19**, 735–745.
27 Y.-H. Zhu, X. Yang, T. Sun, S. Wang, Y.-L. Zhao, J.-M. Yan and X.-B. Zhang, *Electrochem. Energy Rev.*, 2018, **1**, 548–566.
28 S.-H. Chung and A. Manthiram, *Adv. Mater.*, 2019, **31**, 1901125.
29 J.-Y. Hwang, S.-T. Myung and Y.-K. Sun, *Adv. Funct. Mater.*, 2018, **28**, 1802938.
30 X. Zou, P. Xiong, J. Zhao, J. Hu, Z. Liu and Y. Xu, *Phys. Chem. Chem. Phys.*, 2017, **19**, 26495–26506.
31 X. Zhang, D. Yang, X. Rui, Y. Yu and S. Huang, *Curr. Opin. Electrochem.*, 2019, **18**, 24–30.
32 J. Zhang, T. Liu, X. Cheng, M. Xia, R. Zheng, N. Peng, H. Yu, M. Shui and J. Shu, *Nano Energy*, 2019, **60**, 340–361.
33 H. Kim, H. Ji, J. Wang and G. Ceder, *Trends Chem.*, 2019, **1**, 682–692.
34 H. Kim, J. C. Kim, M. Bianchini, D.-H. Seo, J. Rodriguez-Garcia and G. Ceder, *Adv. Energy Mater.*, 2018, **8**, 1702384.
35 J. C. Pramudita, D. Sehrawat, D. Goonetilleke and N. Sharma, *Adv. Energy Mater.*, 2017, **7**, 1602911.
36 V. Gabaudan, L. Monconduit, L. Stievano and R. Berthelot, *Front. Energy Res.*, 2019, **7**, 46.
37 X. Wu, Y. Chen, Z. Xing, C. W. K. Lam, S.-S. Pang, W. Zhang and Z. Ju, *Adv. Energy Mater.*, 2019, **9**, 1900343.
38 X. Wu, D. P. Leonard and X. Ji, *Chem. Mater.*, 2017, **29**, 5031–5042.
39 D. Yang, C. Liu, X. Rui and Q. Yan, *Nanoscale*, 2019, **11**, 15402–15417.
40 M. Chen, Q. Liu, Y. Zhang, G. Xing, S.-L. Chou and Y. Tang, *J. Mater. Chem. A*, 2020, DOI: 10.1039/c9ta11221a.
41 R. Rajagopalan, Y. Tang, X. Ji, C. Jia and H. Wang, *Adv. Funct. Mater.*, 2020, **30**, 1909486.
42 M. Sha, L. Liu, H. Zhao and Y. Lei, *Energy Environ. Mater.*, 2020, **3**, 56–66.
43 C. Zhang, H. Zhao and Y. Lei, *Energy Environ. Mater.*, 2020, **3**, 105–120.
44 T. Hosaka, K. Kubota, A. S. Hameed and S. Komaba, *Chem. Rev.*, 2020, **120**, 6358–6466.
45 J. Ding, H. Zhang, W. Fan, C. Zhong, W. Hu and D. Mitlin, *Adv. Mater.*, 2020, 1908007, DOI: 10.1002/adma.201908007.
46 B. Wang, E. H. Ang, Y. Yang, Y. Zhang, M. Ye, Q. Liu and C. C. Li, *Chem.–Eur. J.*, 2020, DOI: 10.1002/chem.202001811.
47 M. Sha, L. Liu, H. Zhao and Y. Lei, *Carbon Energy*, DOI: 10.1002/cey2.57.
48 R. Boddula and A. M. Asiri, *Potassium-ion Batteries: Materials and Applications*, John Wiley & Sons, 2020.
49 H. Peng, Q. Yu, S. Wang, J. Kim, A. E. Rowan, A. K. Nanjundan, Y. Yamauchi and J. Yu, *Adv. Sci.*, 2019, **6**, 1900431.
50 L. Zhu, G. Ding, L. Xie, X.-Y. Cao, J. Liu, X. Lei and J. Ma, *Chem. Mater.*, 2019, **31**, 8582–8612.
51 C. Han, H. Li, R. Shi, T. Zhang, J. Tong, J. Li and B. Li, *J. Mater. Chem. A*, 2019, **7**, 23378–23415.
52 Q. Zhao, J. Wang, Y. Lu, Y. Li, G. Liang and J. Chen, *Angew. Chem., Int. Ed.*, 2016, **55**, 12528–12532.
53 Z. Song and H. Zhou, *Energy Environ. Sci.*, 2013, **6**, 2280–2301.
54 J. Zhao, J. Yang, P. Sun and Y. Xu, *Electrochem. Commun.*, 2018, **86**, 34–37.
55 B. Li, J. Zhao, Z. Zhang, C. Zhao, P. Sun, P. Bai, J. Yang, Z. Zhou and Y. Xu, *Adv. Funct. Mater.*, 2019, **29**, 1807137.
56 D. Li, W. Tang, C. Wang and C. Fan, *Electrochem. Commun.*, 2019, **105**, 106509.
57 L. Chen, S. Liu, Y. Wang, W. Liu, Y. Dong, Q. Kuang and Y. Zhao, *Electrochim. Acta*, 2019, **294**, 46–52.
58 L. Chen and Y. Zhao, *Mater. Lett.*, 2019, **243**, 69–72.
59 Y. Ding, X. Guo, Y. Qian, L. Zhang, L. Xue, J. B. Goodenough and G. Yu, *Adv. Mater.*, 2019, **31**, 1806956.
60 A. Slesarenko, I. K. Yakuschenko, V. Ramezankhani, V. Sivasankaran, O. Romanyuk, A. V. Mumyatov, I. Zhidkov, S. Tsarev, E. Z. Kurmaev, A. F. Shestakov,

O. V. Yarmolenko, K. J. Stevenson and P. A. Troshin, *J. Power Sources*, 2019, **435**, 226724.
61 S.-Y. Yang, Y.-J. Chen, G. Zhou and Z.-W. Fu, *J. Electrochem. Soc.*, 2018, **165**, A1422–A1429.
62 M. Kato, T. Masese, M. Yao, N. Takeichi and T. Kiyobayashi, *New J. Chem.*, 2019, **43**, 1626–1631.
63 J. Ma, E. Zhou, C. Fan, B. Wu, C. Li, Z.-H. Lu and J. Li, *Chem. Commun.*, 2018, **54**, 5578–5581.
64 Y. Chen, W. Luo, M. Carter, L. Zhou, J. Dai, K. Fu, S. Lacey, T. Li, J. Wan, X. Han, Y. Bao and L. Hu, *Nano Energy*, 2015, **18**, 205–211.
65 Z. Xing, Z. Jian, W. Luo, Y. Qi, C. Bommier, E. S. Chong, Z. Li, L. Hu and X. Ji, *Energy Storage Materials*, 2016, **2**, 63–68.
66 H. Fei, Y. Liu, Y. An, X. Xu, G. Zeng, Y. Tian, L. Ci, B. Xi, S. Xiong and J. Feng, *J. Power Sources*, 2018, **399**, 294–298.
67 L. Fan, R. Ma, J. Wang, H. Yang and B. Lu, *Adv. Mater.*, 2018, **30**, 1805486.
68 Z. Tong, S. Tian, H. Wang, D. Shen, R. Yang and C.-S. Lee, *Adv. Funct. Mater.*, 2019, **30**, 1907656.
69 M. Xiong, W. Tang, B. Cao, C. Yang and C. Fan, *J. Mater. Chem. A*, 2019, **7**, 20127–20131.
70 Y. Hu, W. Tang, Q. Yu, X. Wang, W. Liu, J. Hu and C. Fan, *Adv. Funct. Mater.*, 2020, 2000675, DOI: 10.1002/adfm.202000675.
71 P. Gao, S. Lv, J. Yuan, Z. Chen, H. Shu, X. Yang, E. Liu, S. Tan, M. Ruben, Z. Zhao-Karger and M. Fichtner, *ChemSusChem*, 2020, **13**, 2286.
72 Z. Jian, Y. Liang, I. A. Rodríguez-Pérez, Y. Yao and X. Ji, *Electrochem. Commun.*, 2016, **71**, 5–8.
73 M. Zhou, M. Liu, J. Wang, T. Gu, B. Huang, W. Wang, K. Wang, S. Cheng and K. Jiang, *Chem. Commun.*, 2019, **55**, 6054–6057.
74 M. Tang, Y. Wu, Y. Chen, C. Jiang, S. Zhu, S. Zhuo and C. Wang, *J. Mater. Chem. A*, 2019, **7**, 486–492.
75 Y. Hu, H. Ding, Y. Bai, Z. Liu, S. Chen, Y. Wu, X. Yu, L. Fan and B. Lu, *ACS Appl. Mater. Interfaces*, 2019, **11**, 42078–42085.
76 B. Tian, J. Zheng, C. Zhao, C. Liu, C. Su, W. Tang, X. Li and G.-H. Ning, *J. Mater. Chem. A*, 2019, **7**, 9997–10003.
77 R. R. Kapaev, I. S. Zhidkov, E. Z. Kurmaev, K. J. Stevenson and P. A. Troshin, *J. Mater. Chem. A*, 2019, **7**, 22596–22603.
78 R. R. Kapaev, F. A. Obrezkov, K. J. Stevenson and P. A. Troshin, *Chem. Commun.*, 2019, **55**, 11758–11761.
79 H. Gao, L. Xue, S. Xin and J. B. Goodenough, *Angew. Chem., Int. Ed.*, 2018, **57**, 5449–5453.
80 L. Fan, Q. Liu, Z. Xu and B. Lu, *ACS Energy Lett.*, 2017, **2**, 1614–1620.
81 F. A. Obrezkov, A. F. Shestakov, V. F. Traven, K. J. Stevenson and P. A. Troshin, *J. Mater. Chem. A*, 2019, **7**, 11430–11437.
82 F. A. Obrezkov, V. Ramezankhani, I. Zhidkov, V. F. Traven, E. Z. Kurmaev, K. J. Stevenson and P. A. Troshin, *J. Phys. Chem. Lett.*, 2019, **10**, 5440–5445.
83 C. Li, J. Xue, A. Huang, J. Ma, F. Qing, A. Zhou, Z. Wang, Y. Wang and J. Li, *Electrochim. Acta*, 2019, **297**, 850–855.
84 H. Chen, Z. Zhang, Z. Wei, G. Chen, X. Yang, C. Wang and F. Du, *Sustainable Energy Fuels*, 2020, **4**, 128–131.
85 Y. Bai, W. Fu, W. Chen, Z. Chen, X. Pan, X. Lv, J. Wu and X. Pan, *J. Mater. Chem. A*, 2019, **7**, 24454–24461.
86 L. Jiang, Y. Lu, C. Zhao, L. Liu, J. Zhang, Q. Zhang, X. Shen, J. Zhao, X. Yu, H. Li, X. Huang, L. Chen and Y.-S. Hu, *Nat. Energy*, 2019, **4**, 495–503.
87 K. Lei, F. Li, C. Mu, J. Wang, Q. Zhao, C. Chen and J. Chen, *Energy Environ. Sci.*, 2017, **10**, 552–557.
88 J. Liao, Q. Hu, Y. Yu, H. Wang, Z. Tang, Z. Wen and C. Chen, *J. Mater. Chem. A*, 2017, **5**, 19017–19024.
89 Y. Luo, L. Liu, K. Lei, J. Shi, G. Xu, F. Li and J. Chen, *Chem. Sci.*, 2019, **10**, 2048–2052.
90 Q. Deng, J. Pei, C. Fan, J. Ma, B. Cao, C. Li, Y. Jin, L. Wang and J. Li, *Nano Energy*, 2017, **33**, 350–355.
91 X. Wang, K. Han, C. Wang, Z. Liu, X. Xu, M. Huang, P. Hu, J. Meng, Q. Li and L. Mai, *Chem. Commun.*, 2018, **54**, 11029–11032.
92 C. Wang, W. Tang, Z. Yao, Y. Chen, J. Pei and C. Fan, *Org. Electron.*, 2018, **62**, 536–541.
93 C. Li, X. Hu and B. Hu, *Electrochim. Acta*, 2017, **253**, 439–444.
94 C. Fan, M. Zhao, C. Li, C. Wang, B. Cao, X. Chen, Y. Li and J. Li, *Electrochim. Acta*, 2017, **253**, 333–338.
95 Q. Deng, S. Feng, P. Hui, H. Chen, C. Tian, R. Yang and Y. Xu, *J. Alloys Compd.*, 2020, 154714, DOI: 10.1016/j.jallcom.2020.154714.
96 C. Li, Q. Deng, H. Tan, C. Wang, C. Fan, J. Pei, B. Cao, Z. Wang and J. Li, *ACS Appl. Mater. Interfaces*, 2017, **9**, 27414–27420.
97 C. Li, J. Xue, J. Ma and J. Li, *J. Electrochem. Soc.*, 2019, **166**, A5221–A5225.
98 C. Wang, W. Tang, Z. Yao, B. Cao and C. Fan, *Chem. Commun.*, 2019, **55**, 1801–1804.
99 Y. Liang, C. Luo, F. Wang, S. Hou, S.-C. Liou, T. Qing, Q. Li, J. Zheng, C. Cui and C. Wang, *Adv. Energy Mater.*, 2019, **9**, 1802986.
100 Y. Zhu, P. Chen, Y. Zhou, W. Nie and Y. Xu, *Electrochim. Acta*, 2019, **318**, 262–271.
101 Q. Xue, D. Li, Y. Huang, X. Zhang, Y. Ye, E. Fan, L. Li, F. Wu and R. Chen, *J. Mater. Chem. A*, 2018, **6**, 12559–12564.
102 Y. Liang, Y. Jing, S. Gheytani, K.-Y. Lee, P. Liu, A. Facchetti and Y. Yao, *Nat. Mater.*, 2017, **16**, 841–848.
103 M. Wang, H. Wang, H. Zhang and X. Li, *J. Energy Chem.*, 2020, **48**, 14–20.
104 C. Zhang, Y. Qiao, P. Xiong, W. Ma, P. Bai, X. Wang, Q. Li, J. Zhao, Y. Xu, Y. Chen, J. H. Zeng, F. Wang, Y. Xu and J.-X. Jiang, *ACS Nano*, 2019, **13**, 745–754.
105 X. Chen, H. Zhang, C. Ci, W. Sun and Y. Wang, *ACS Nano*, 2019, **13**, 3600–3607.
106 S.-Y. Li, W.-H. Li, X.-L. Wu, Y. Tian, J. Yue and G. Zhu, *Chem. Sci.*, 2019, **10**, 7695–7701.
107 H. Zhang, W. Sun, X. Chen and Y. Wang, *ACS Nano*, 2019, **13**, 14252–14261.
108 G. Zeng, Y. An, H. Fei, T. Yuan, S. Qing, L. Ci, S. Xiong and J. Feng, *Funct. Mater. Lett.*, 2018, **11**, 1840003.
109 T. Sun, Z.-J. Li, X. Yang, S. Wang, Y.-H. Zhu and X.-B. Zhang, *Chin. Chem. Soc*, 2019, **1**, 365–372.
110 R. R. Kapaev, I. S. Zhidkov, E. Z. Kurmaev, K. J. Stevenson and P. A. Troshin, *Chem. Commun.*, 2020, **56**, 1541–1544.

111 K. Chihara, N. Chujo, A. Kitajou and S. Okada, *Electrochim. Acta*, 2013, **110**, 240–246.
112 G.-M. Weng, Y. Xie, H. Wang, C. Karpovich, J. Lipton, J. Zhu, J. Kong, L. D. Pfefferle and A. D. Taylor, *Angew. Chem., Int. Ed.*, 2019, **58**, 13727–13733.
113 M. Lee, J. Hong, J. Lopez, Y. Sun, D. Feng, K. Lim, W. C. Chueh, M. F. Toney, Y. Cui and Z. Bao, *Nat. Energy*, 2017, **2**, 861–868.
114 X. Guo, L. Zhang, Y. Ding, J. B. Goodenough and G. Yu, *Energy Environ. Sci.*, 2019, **12**, 2605–2619.
115 M. Kato, K.-i. Senoo, M. Yao and Y. Misaki, *J. Mater. Chem. A*, 2014, **2**, 6747–6754.
116 C. Fang, Y. Huang, L. Yuan, Y. Liu, W. Chen, Y. Huang, K. Chen, J. Han, Q. Liu and Y. Huang, *Angew. Chem.*, 2017, **129**, 6897–6901.
117 S. Renault, V. A. Mihali, K. Edström and D. Brandell, *Electrochem. Commun.*, 2014, **45**, 52–55.
118 Y. Huang, R. Yuan and S. Zhou, *J. Mater. Chem.*, 2012, **22**, 883–888.
119 W. Deng, Y. Shen, J. Qian, Y. Cao and H. Yang, *ACS Appl. Mater. Interfaces*, 2015, **7**, 21095–21099.
120 C. Peng, G.-H. Ning, J. Su, G. Zhong, W. Tang, B. Tian, C. Su, D. Yu, L. Zu, J. Yang, M.-F. Ng, Y.-S. Hu, Y. Yang, M. Armand and K. P. Loh, *Nat. Energy*, 2017, **2**, 17074.
121 M. Mao, C. Luo, T. P. Pollard, S. Hou, T. Gao, X. Fan, C. Cui, J. Yue, Y. Tong, G. Yang, T. Deng, M. Zhang, J. Ma, L. Suo, O. Borodin and C. Wang, *Angew. Chem., Int. Ed.*, 2019, **58**, 17820.
122 G. Liao, Q. Li and Z. Xu, *Prog. Org. Coat.*, 2019, **126**, 35–43.
123 Y. Fang, M. O. Senge, E. Van Caemelbecke, K. M. Smith, C. J. Medforth, M. Zhang and K. M. Kadish, *Inorg. Chem.*, 2014, **53**, 10772–10778.
124 A. Ghosh, I. Halvorsen, H. J. Nilsen, E. Steene, T. Wondimagegn, R. Lie, E. van Caemelbecke, N. Guo, Z. Ou and K. M. Kadish, *J. Phys. Chem. B*, 2001, **105**, 8120–8124.
125 S. M. LeCours, S. G. DiMagno and M. J. Therien, *J. Am. Chem. Soc.*, 1996, **118**, 11854–11864.
126 P. Poizot, F. Dolhem and J. Gaubicher, *Curr. Opin. Electrochem.*, 2018, **9**, 70–80.
127 X. Dong, H. Yu, Y. Ma, J. L. Bao, D. G. Truhlar, Y. Wang and Y. Xia, *Chem.–Eur. J.*, 2017, **23**, 2560–2565.
128 S. Perticarari, E. Grange, T. Doizy, Y. Pellegrin, E. Quarez, K. Oyaizu, A. J. Fernandez-Ropero, D. Guyomard, P. Poizot, F. Odobel and J. Gaubicher, *Chem. Mater.*, 2019, **31**, 1869–1880.
129 H. Glatz, E. Lizundia, F. Pacifico and D. Kundu, *ACS Appl. Energy Mater.*, 2019, **2**, 1288–1294.
130 F. Wan, L. Zhang, X. Wang, S. Bi, Z. Niu and J. Chen, *Adv. Funct. Mater.*, 2018, **28**, 1804975.
131 Y. Zhang, Y. An, B. Yin, J. Jiang, S. Dong, H. Dou and X. Zhang, *J. Mater. Chem. A*, 2019, **7**, 11314–11320.
132 K. Chihara, A. Katogi, K. Kubota and S. Komaba, *Chem. Commun.*, 2017, **53**, 5208–5211.
133 A. S. Hameed, A. Katogi, K. Kubota and S. Komaba, *Adv. Energy Mater.*, 2019, **9**, 1902528.
134 X. Bie, K. Kubota, T. Hosaka, K. Chihara and S. Komaba, *J. Mater. Chem. A*, 2017, **5**, 4325–4330.
135 Z. Shadike, D.-R. Shi, W. Tian, M.-H. Cao, S.-F. Yang, J. Chen and Z.-W. Fu, *J. Mater. Chem. A*, 2017, **5**, 6393–6398.
136 S. Chong, Y. Wu, S. Guo, Y. Liu and G. Cao, *Energy Storage Materials*, 2019, **22**, 120–127.
137 X. Wang, X. Xu, C. Niu, J. Meng, M. Huang, X. Liu, Z. Liu and L. Mai, *Nano Lett.*, 2017, **17**, 544–550.
138 Y.-H. Zhu, Q. Zhang, X. Yang, E.-Y. Zhao, T. Sun, X.-B. Zhang, S. Wang, X.-Q. Yu, J.-M. Yan and Q. Jiang, *Chem*, 2019, **5**, 168–179.
139 M. Clites, J. L. Hart, M. L. Taheri and E. Pomerantseva, *ACS Energy Lett.*, 2018, **3**, 562–567.
140 N.-C. Lai, G. Cong and Y.-C. Lu, *J. Mater. Chem. A*, 2019, **7**, 20584–20589.
141 X. Yu and A. Manthiram, *Energy Storage Materials*, 2018, **15**, 368–373.
142 C. Yang, J. Chen, X. Ji, T. P. Pollard, X. Lü, C.-J. Sun, S. Hou, Q. Liu, C. Liu, T. Qing, Y. Wang, O. Borodin, Y. Ren, K. Xu and C. Wang, *Nature*, 2019, **569**, 245–250.
143 C. L. Yaws and D. H. Chen, in *Thermophysical Properties of Chemicals and Hydrocarbons*, ed. C. L. Yaws, William Andrew Publishing, Norwich, NY, 2009, pp. 207–295, DOI: 10.1016/b978-081551596-8.50010-9.
144 H. Tan, X. Du, J.-Q. Huang and B. Zhang, *Chem. Commun.*, 2019, **55**, 11311–11314.
145 C. L. Yaws and D. H. Chen, in *Thermophysical Properties of Chemicals and Hydrocarbons*, ed. C. L. Yaws, William Andrew Publishing, Norwich, NY, 2009, pp. 296–308, DOI: 10.1016/b978-081551596-8.50011-0.
146 Y. Lu, Q. Zhang, L. Li, Z. Niu and J. Chen, *Chem*, 2018, **4**, 2786–2813.
147 W. Huang, Z. Zhu, L. Wang, S. Wang, H. Li, Z. Tao, J. Shi, L. Guan and J. Chen, *Angew. Chem., Int. Ed.*, 2013, **52**, 9162–9166.
148 T. Hosaka, K. Kubota, H. Kojima and S. Komaba, *Chem. Commun.*, 2018, **54**, 8387–8390.
149 L. Qin, N. Xiao, J. Zheng, Y. Lei, D. Zhai and Y. Wu, *Adv. Energy Mater.*, 2019, **9**, 1902618.
150 N. Xiao, W. D. McCulloch and Y. Wu, *J. Am. Chem. Soc.*, 2017, **139**, 9475–9478.
151 T. Hosaka, S. Muratsubaki, K. Kubota, H. Onuma and S. Komaba, *J. Phys. Chem. Lett.*, 2019, **10**, 3296–3300.
152 L. Qin, Y. Lei, H. Wang, J. Dong, Y. Wu, D. Zhai, F. Kang, Y. Tao and Q.-H. Yang, *Adv. Energy Mater.*, 2019, **9**, 1901427.
153 H. Wang, J. Hu, J. Dong, K. C. Lau, L. Qin, Y. Lei, B. Li, D. Zhai, Y. Wu and F. Kang, *Adv. Energy Mater.*, 2019, **9**, 1902697.
154 L. Zhang, S. Peng, Y. Ding, X. Guo, Y. Qian, H. Celio, G. He and G. Yu, *Energy Environ. Sci.*, 2019, **12**, 1989–1998.
155 R. Kleerebezem, J. Mortier, L. W. Hulshoff Pol and G. Lettinga, *Water Sci. Technol.*, 1997, **36**, 237–248.
156 R. D. Sheehan, *Ullmann's Encyclopedia of Industrial Chemistry*, 2000, Wiley, DOI: 10.1002/14356007.a26_193.
157 C. Luo, G.-L. Xu, X. Ji, S. Hou, L. Chen, F. Wang, J. Jiang, Z. Chen, Y. Ren, K. Amine and C. Wang, *Angew. Chem., Int. Ed.*, 2018, **57**, 2879–2883.

158 C. Luo, X. Ji, S. Hou, N. Eidson, X. Fan, Y. Liang, T. Deng, J. Jiang and C. Wang, *Adv. Mater.*, 2018, **30**, 1706498.
159 C. Luo, X. Ji, J. Chen, K. J. Gaskell, X. He, Y. Liang, J. Jiang and C. Wang, *Angew. Chem., Int. Ed.*, 2018, **57**, 8567–8571.
160 C. Luo, O. Borodin, X. Ji, S. Hou, K. J. Gaskell, X. Fan, J. Chen, T. Deng, R. Wang, J. Jiang and C. Wang, *Proc. Natl. Acad. Sci. U. S. A.*, 2018, **115**, 2004–2009.
161 Y. Ding, Y. Li and G. Yu, *Chem*, 2016, **1**, 790–801.
162 Y. Liang, P. Zhang, S. Yang, Z. Tao and J. Chen, *Adv. Energy Mater.*, 2013, **3**, 600–605.
163 Y. R. Beg, G. R. Nishad, C. Das and P. Singh, in *Conducting Polymers-Based Energy Storage Materials*, ed. D. Inamuddin, R. Boddula, M. F. Ahmer and A. M. Asiri, CRC Press, Boca Raton, 1st edn, 2019, pp. 1–50, DOI: 10.1201/9780429202261.
164 L. Fan, R. Ma, Q. Zhang, X. Jia and B. Lu, *Angew. Chem., Int. Ed.*, 2019, **58**, 10500–10505.
165 Y. Cui, W. Liu, X. Wang, J. Li, Y. Zhang, Y. Du, S. Liu, H. Wang, W. Feng and M. Chen, *ACS Nano*, 2019, **13**, 11582–11592.
166 Y. An, Y. Tian, Y. Li, S. Xiong, G. Zhao, J. Feng and Y. Qian, *J. Mater. Chem. A*, 2019, **7**, 21966–21975.
167 K. Lei, C. Wang, L. Liu, Y. Luo, C. Mu, F. Li and J. Chen, *Angew. Chem., Int. Ed.*, 2018, **57**, 4687–4691.
168 H. Yang, R. Xu, Y. Yao, S. Ye, X. Zhou and Y. Yu, *Adv. Funct. Mater.*, 2019, **29**, 1809195.
169 J. Zheng, Y. Yang, X. Fan, G. Ji, X. Ji, H. Wang, S. Hou, M. R. Zachariah and C. Wang, *Energy Environ. Sci.*, 2019, **12**, 615–623.
170 N. Cheng, J. Zhao, L. Fan, Z. Liu, S. Chen, H. Ding, X. Yu, Z. Liu and B. Lu, *Chem. Commun.*, 2019, **55**, 12511–12514.
171 Y. Zhao, J. Zhu, S. J. H. Ong, Q. Yao, X. Shi, K. Hou, Z. J. Xu and L. Guan, *Adv. Energy Mater.*, 2018, **8**, 1802565.
172 Y. Wu, S. Hu, R. Xu, J. Wang, Z. Peng, Q. Zhang and Y. Yu, *Nano Lett.*, 2019, **19**, 1351–1358.
173 Z. Li, J. Huang, B. Yann Liaw, V. Metzler and J. Zhang, *J. Power Sources*, 2014, **254**, 168–182.
174 S. S. Zhang, K. Xu and T. R. Jow, *J. Power Sources*, 2006, **160**, 1349–1354.
175 Z. Chen, I. Belharouak, Y.-K. Sun and K. Amine, *Adv. Funct. Mater.*, 2013, **23**, 959–969.
176 S. Xu, Y. Chen and C. Wang, *J. Mater. Chem. A*, 2020, DOI: 10.1039/d0ta03310c.